Fatigue: A Complex Subject—Some Simple Approximations

Both ends of the fatigue spectrum are covered in this lecture. On the one hand, the present state of understanding of the mechanism is reviewed and the complexity of the process observed. On the other hand, some approximations useful in design are outlined and their application illustrated

by S. S. Manson

FOREWORD—It was my privilege to serve on the Executive Committee of the Society for Experimental Stress Analysis in 1951 when this lectureship was first inaugurated. Normally our concern was largely with financial matters but, at this meeting, our subject of discussion was much more pleasurable—how could we be of greater service to the membership of the Society and to the technical community at large? One of the members of the committee suggested that it was about time—we were then 8 years old—to institute an honorary lectureship within the Society. This sounded like a very good idea, and we were about to embark on a discussion as to how it would be designated. Frankly my thoughts turned in the direction of some elderly hero of the past in the field of stress analysis. I did not think at all along the lines of one of the other members who sat next to me and said, "How about Bill Murray?" Bill was not in the room at the time. After the suggestion was made, however, it seemed like the only possible idea. I wondered how I could ever have thought in any direction other than that. Bill was a founder, he was our first president, he was the executive secretary and our treasurer. Between meetings he was the entire Society and did all of the work, including editing of the "*Proceedings*." He did this on donated time without remuneration. So the suggestion not only made sense, but it really was the only right thing to do. By the time Bill came back, there was no need for discussion. I did not need to be convinced and neither did anyone else. The decision was unanimous; it was to be the William M. Murray Lecture. We asked Bill if he would give the first lecture, and, of course, he did. In so doing, he set a standard of excellence that has been followed ever since. The twelve Murray lectures that have been given in the ensuing years have all been a true credit to the Society. It is indeed a privilege to take a place among those honoring Bill, and it is my hope that the lecture that I shall present to you will in small measure, at least, follow the high standards that have already been set.

S. S. Manson is Chief of Materials and Structures Division, Lewis Research Center, National Aeronautics and Space Administration, Cleveland, Ohio.

Lecture was presented at 1964 SESA Annual Meeting held in Cleveland, Ohio, on October 28–30.

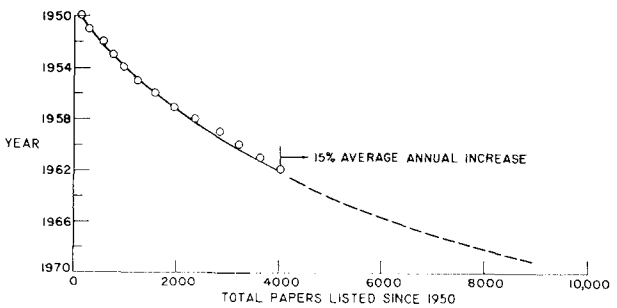

Fig. 1—Selected publications on fatigue (from ASTM references on fatigue)

Introduction

I have chosen as the subject of this lecture: fatigue—some of its complexities, some simplifications. This subject is not a neglected one; Fig. 1 shows, for example, a plot of the number of reports that have appeared since 1950 relating to fatigue. Actually, the literature goes back 100 years, but even if we start in 1950, we see how vast it is. The references cited here are selected papers listed by the ASTM; it is not a complete compilation of all publications. Since the last listing was in 1962, I have extrapolated the curve for a few ensuing years based on the "rule of thumb" given by the ASTM that, on the average, the papers increase at a rate of 15 percent per year. This method of presentation is fashioned after an approach suggested in a private communication by Professors Burns and Morrison of the University of London, and, I believe, particularly appropriate for students of fatigue. It is quite clear that, if a person wished

Fig. 2—Factors associated with fatigue studies

to keep up with the literature and read one report per working day, he would fall behind on the order of 1 year for every year that he read. This would be true if he started with a knowledge of the existing literature; catching up on the backlog would be almost impossible. In the characteristic fashion of fatigue, we seem to be approaching an endurance limit—a time after which keeping abreast will be virtually impossible.

Just why there are so many reports on this subject is indicated in Fig. 2. We see the tremendous number of facets it presents, some independent of each other, some interrelated and some being merely alternate expressions identifying the same factor. Despite the many investigations that have been made, generalities seem quite elusive, and studies of the basic fatigue mechanism, investigations of the many phenomena involving engineering data, and final component testing, will continue to attract the attention of many investigators and result in many reports. When I undertook to prepare this lecture, it was my intention to provide at least a "thumb-nail" description of the state of the art regarding the basic phenomenon. I had intended to show first how complex it was, and then proceed to indicate some simple but useful approximations that were evolved in recent years. I found, however, that even a cursory survey would involve such lengthy discussion that it would be inappropriate for the limited time available. Furthermore, so many excellent references have appeared in recent years outlining our state of understanding on the fundamental aspects of fatigue, that I would, in the main, be repeating, largely with less qualification, the words of these excellent authors.[1–4] My discussion will limit

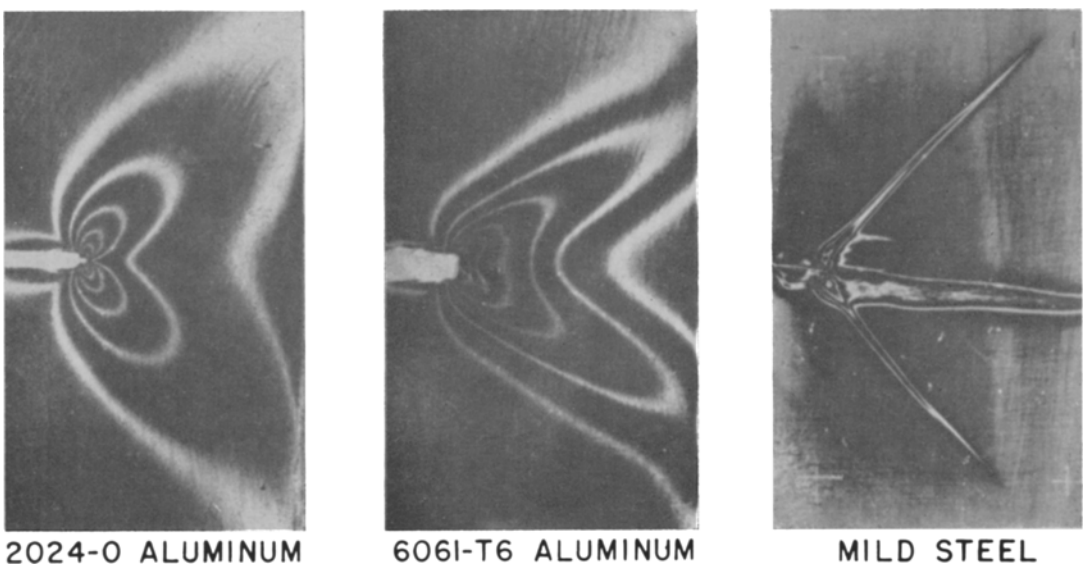

Fig. 3—Photoelastic-coating method to determine strain distribution at notch tip. (W. W. Gerberich, 1963)

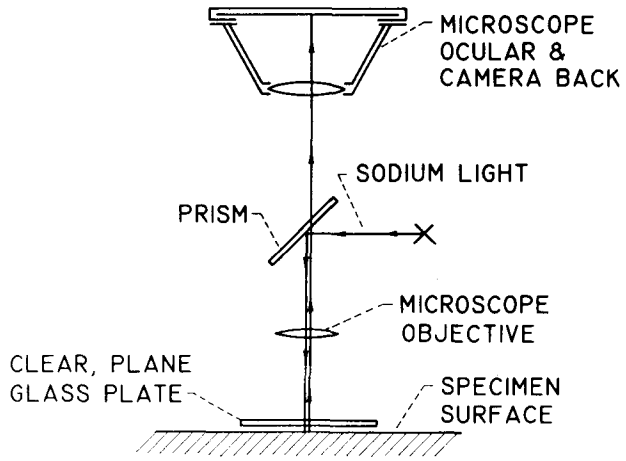

SCHEMATIC OF OPTICS FOR OBSERVING PHASE-INTERFERENCE FRINGES

SPECIMEN UNDER HIGH TENSILE LOAD

Fig. 4—Phase-interference method to determine strain distribution at notch tip. (G. U. Oppel and P. W. Hill, 1964)

itself, therefore, to those fundamental aspects that relate specifically to investigations that have been conducted in our laboratory at Lewis Research Center, or those which elucidate some details pertinent to the discussion of our results. For this reason, the results of our experiments will be described first, and the fundamental aspects reserved until the terminal section.

Before proceeding, however, to a discussion of experimental results and their significance, it is appropriate to mention several of the new tools that have recently been arrayed toward obtaining an understanding of the fatigue phenomenon. This is appropriate because this Society is, after all, devoted to experimental matters.

Some Recent Experimental Tools and Techniques

Since fatigue is so intimately related to the question of generating and propagating a crack, and since the photoelastic technique really comes into its own when studying stress distribution in the vicinity of a crack, it is very logical that this research tool should have contributed to our understanding of fatigue. Figure 3 shows some results that have been presented by Gerberich[5] showing the strain distribution at the tip of a notch. The photoelastic-coating method is especially valuable here because it enables us to study the strain distribution in metallic materials.

The phase-interference method has also been applied to study stress distribution in the vicinity of a notch tip. Figure 4 is taken from a SESA publication in which Oppel and Hill[6] have presented their results using this technique. Briefly, light is directed through an optical system onto an initially flat surface of the specimen. In the undeformed condition of the specimen, the plate glass is parallel to the specimen surface. Deformation of the specimen by loading causes a variation

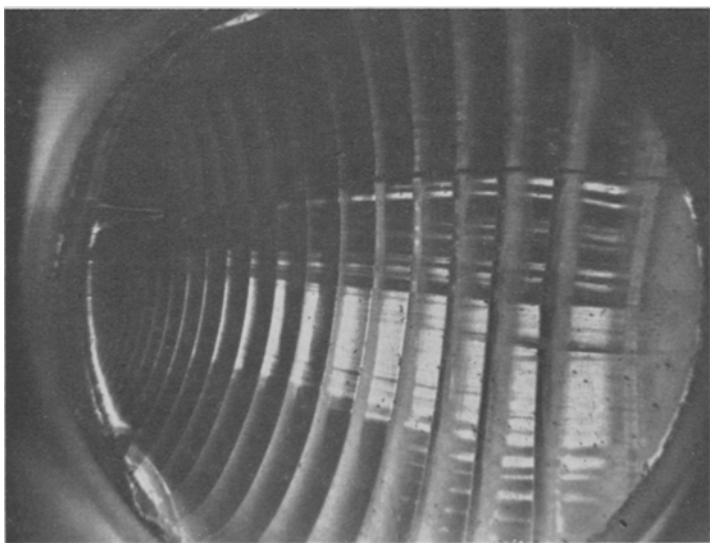

Fig. 5—Crack-growth striations on fracture surface of $^1/_4$-in. diam polycarbonate-resin specimen; 115 cycles to fracture

in the distance between the plate glass and the specimen at different points, and results in a pattern very similar to Newton's rings, such as that shown on the right in the figure.

Figure 5 shows another technique that has been used in our own laboratory. It makes use of a polycarbonate resin, a plastic material, which, when fatigued, clearly shows striations. Each of these striations provides an indication of the distance that the crack has progressed from one cycle to the next. Most specifically, our interest is in how the fatigue crack gets started and how it grows during the very early stages. The use of this material permits the visual observations of the progression of cracks without a microscope. We shall refer later to some results obtained in our laboratory making use of this technique.

Figure 6 refers to another very valuable tool that has been adopted by investigators in fatigue

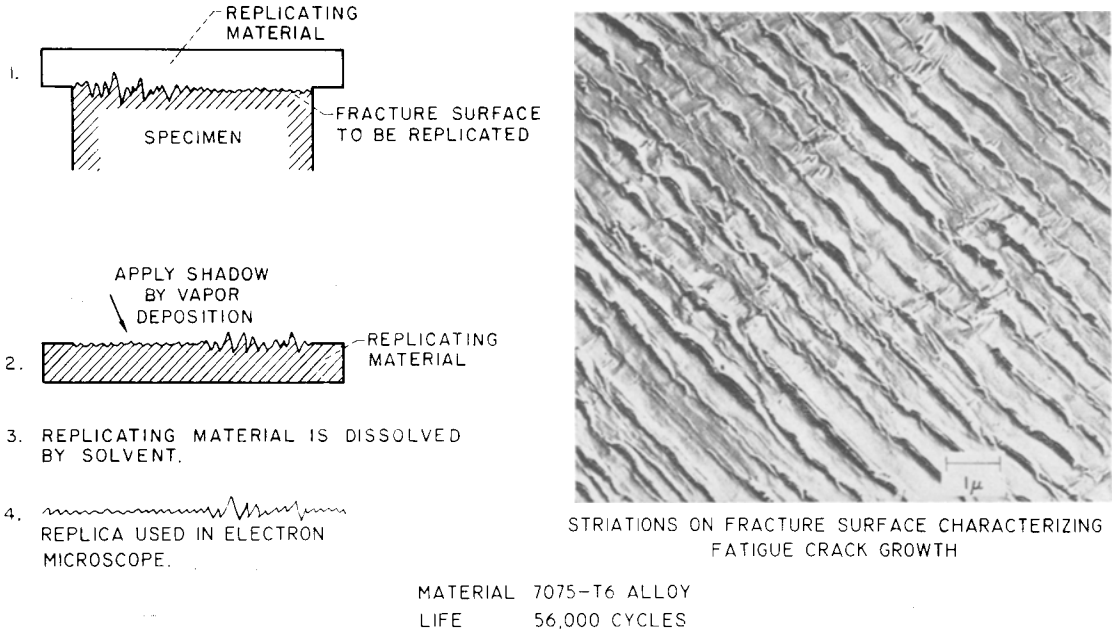

Fig. 6—Electron-microscopy studies of fatigue-fracture surface by replication. Material: 7075-T6 alloy; life: 56,000 cycles. (Bedesem and Harrell—NASA)

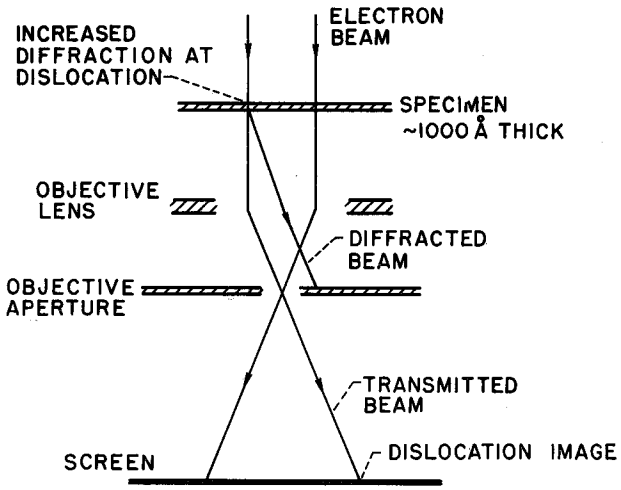

Fig. 7—Formation of dislocation image by transmission electron microscopy. (Howie and Whelan, 1961)

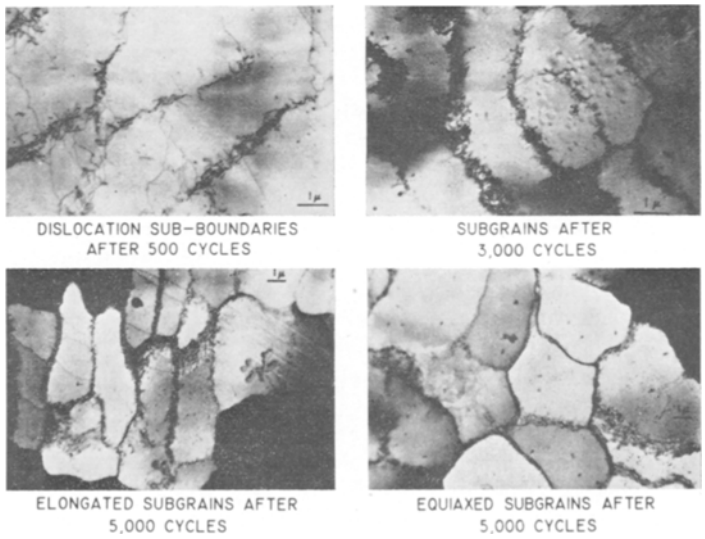

Fig. 8—Use of transmission electron microscopy to observe formation of substructure in aluminum. Total strain range, 0.004; life $\approx 5 \times 10^5$ cycles. (Grosskreutz, 1963)

within the last decade. This tool is the electron microscope, whereby very high magnifications can be accomplished, making it possible to observe the closely spaced individual striations during fatigue-crack growth of long-life specimens. This figure shows the striations that have been observed by Bedesem and Harrell of our laboratory in a study of the aluminum alloy 7075-T6. Every ripple represents the growth of the crack during a cycle of loading. In this case, the crack per cycle is of the order of 30 μin. Such patterns are made by covering the surface with a plastic replicating material, as shown in the upper left of the figure. The plastic material is then stripped off the specimen, leaving an exact replica of the surface topography. This surface is then shadowed by the use of carbon, or other materials such as germanium, which forms an extremely thin film having the shape of the surface. Shadowing at an angle produces highlights that make it possible to distinguish regions of surface depression from those of elevation. The plastic replica is then removed and the thin carbon or metallic film is studied in the electron microscope.

Figure 7 shows another approach involving transmission electron microscopy.[7] Here the specimen itself, rather than a replica of the surface, is placed in the microscope. To be penetrated by the electron beam, however, the specimen must be very thin. The layers of atoms act as a diffraction

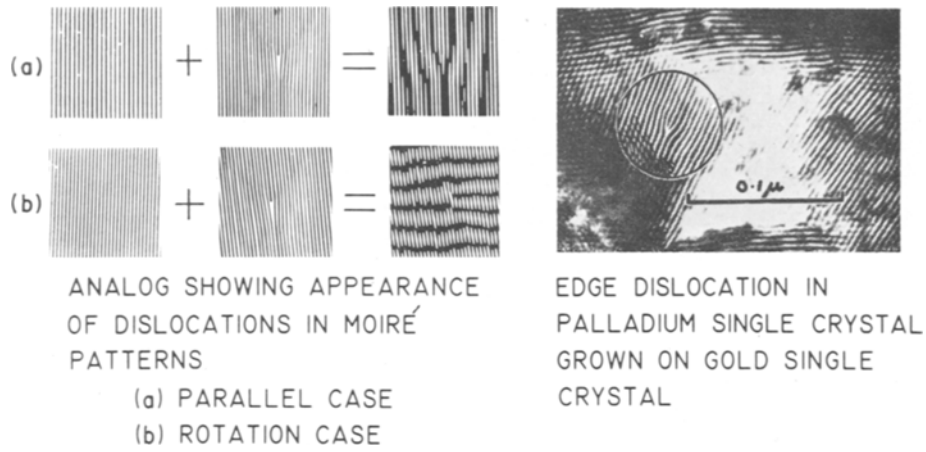

Fig. 9—Moiré method used to observe dislocations in crystal lattice by electron microscopy. (J. W. Menter, 1958)

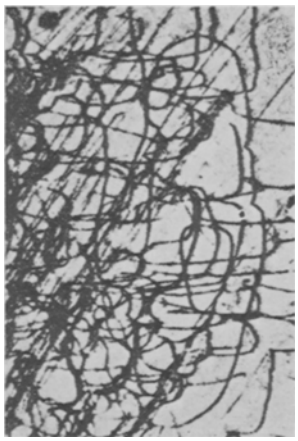

Fig. 10—Observation of dislocations in silicon by X-ray diffraction. (A. R. Lang, 1959)

grating, and any disarray in the lattice is indicated by the pattern generated by the electron beam on the screen. A typical pattern is shown in Fig. 8 taken from the work of Grosskreutz.[8] The dark regions are dislocations—regions of atomic disarray—and it is seen from the photographs how the grains break up into a number of smaller regions called subgrains, separated from each other by dislocation networks. Since this method involves the use of very thin films of the specimen itself, it is sometimes questioned whether the behavior of such films is typical of the behavior of bulk material. Much needs to be done to resolve the questions that have been raised regarding the applicability of the results obtained by these investigations. It is clear, however, that this technique can be extremely useful.

A combination of the technique involving the use of the electron microscope and the moiré method is illustrated in Fig. 9.[9] Here a very thin layer of a single crystal of palladium was deposited on a correspondingly thin single crystal of gold. The array of atoms in each of these crystals constituted the grids that combined to form a moiré pattern. The interference pattern produced by the grids was observed with an electron microscope. In this figure, one of the grids is assumed to be perfect and the other to contain a dislocation. The moiré pattern that results is distinguishable by means of the electron microscope, whereas the actual atomic array of the materials themselves is too fine to be resolved in this manner. Thus, by this method, it is possible to observe disarrays in the atomic structure such as the edge dislocation shown at the right of the figure.

X-rays are an alternate means of detecting disarray in a crystal lattice, since the lattice will diffract the X-rays in much the same manner as an electron beam. Thus, using very thin films of crystalline materials in which the lattice arrangements are not perfect and bombarding these with an X-ray beam result in photographs similar to that shown in Fig. 10.[10] This figure shows a very complicated array of dislocations in silicon, as brought out by the use of X-ray diffraction.

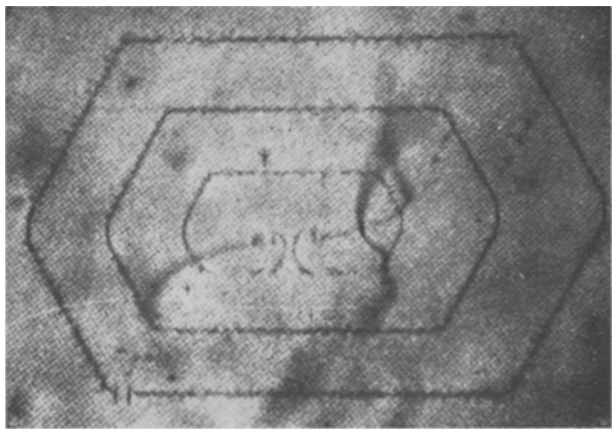

Fig. 11—Observation of dislocations by decoration. Frank-Read source in silicon observed using copper decoration. (W. C. Dash, 1957)

Decoration and etching techniques have been used to provide photographic evidence of the existence of dislocations and their geometric properties. Figure 11 shows a classic photograph obtained by Dash[11] of a Frank-Read source using copper decoration. The development of etch pits is now a well-established technique. Recently, a very interesting innovation has been developed by Hahn and Rosenfeld[12]; by using a silicon steel and a special etchant, they were able to bring out in bold contrast the regions of plastic flow in the vicinity of a notch. Figure 12 shows some of their results. A sheet with a notch was subjected to loading, and the region of plastic flow was first observed by this technique at the surface. By machining away half of the specimen and then etching the midsection, the distribution of plastic flow in the midsection of the plate was made apparent. Note the difference in appearance of these regions. Such studies can be extremely useful in understanding the role of plastic flow and the effect of constraint of such plastic flow on the generation of cracks.

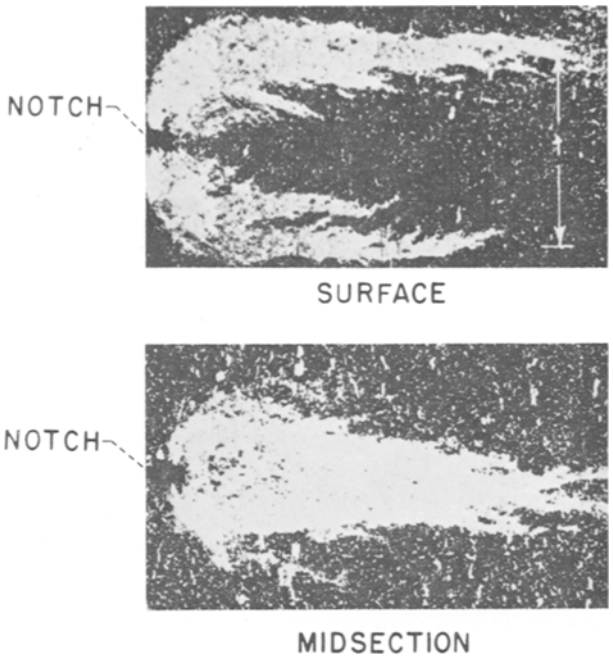

Fig. 12—Etching techniques to reveal plastic zone. (Hahn and Rosenfield, 1964)

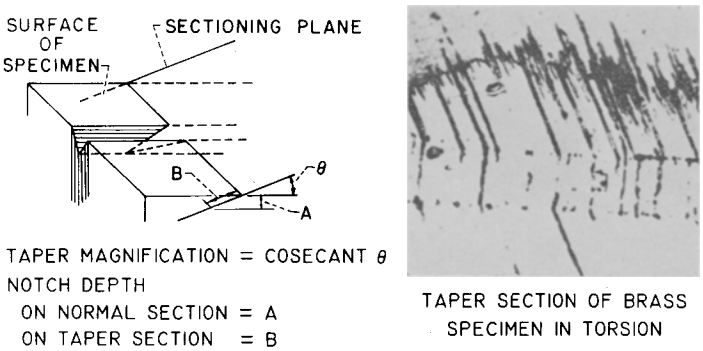

Fig. 13—Observation of fatigue damage at specimen surface by taper sectioning. (W. A. Wood, et al., 1963)

Another technique that has been quite useful in studying the cracks generated by fatigue is called "taper sectioning," and it is illustrated in Fig. 13. Here the attempt is made to observe a very shallow crack by taking advantage of the geometric fact that, if the surface is cut by a plane that makes a very small angle with it, the shallow crack will be elongated in accordance with the cosecant relation of the angle between the cutting plane and the surface. Although the figure shows this angle θ to be of appreciable magnitude, so as to be geometrically distinguishable, the angle is made very small in practice so that the magnification achieved is quite large, of the order of 20. In this way, cracks that are hardly distinguishable become evident when "taper sectioning" is applied. It is evident that a distortion of the geometry results because the magnification occurs only in the depth of crack, but not in the width; thus, care must be exercised in interpreting the results of such studies. A taper section of a brass specimen tested in torsion is shown on the right of Fig. 13.[13]

Another approach that can be used in the study of crack propagation is shown in Fig. 14; it makes use of ultrasonic techniques and has been under investigation in our laboratory by Klima, Lesco and Freche. By this technique, it has been possible to detect cracks less than 0.003 in. long in notched sheet specimens. As a matter of interest, it should be noted that cracks were detected well within the first 10 percent of the life of a *notched* specimen. The question of crack initiation in smooth specimens will be taken up later.

The foregoing techniques are certainly not the only ones that have been brought to bear on this problem of fatigue. Among others are acoustic emission, exo-electron emission, vacuum studies, magnetic effects, resistance effects, damping, heat conduction, thermographic studies, optical microscopes, cinematography and many others. By far, the most powerful tool is the process of human

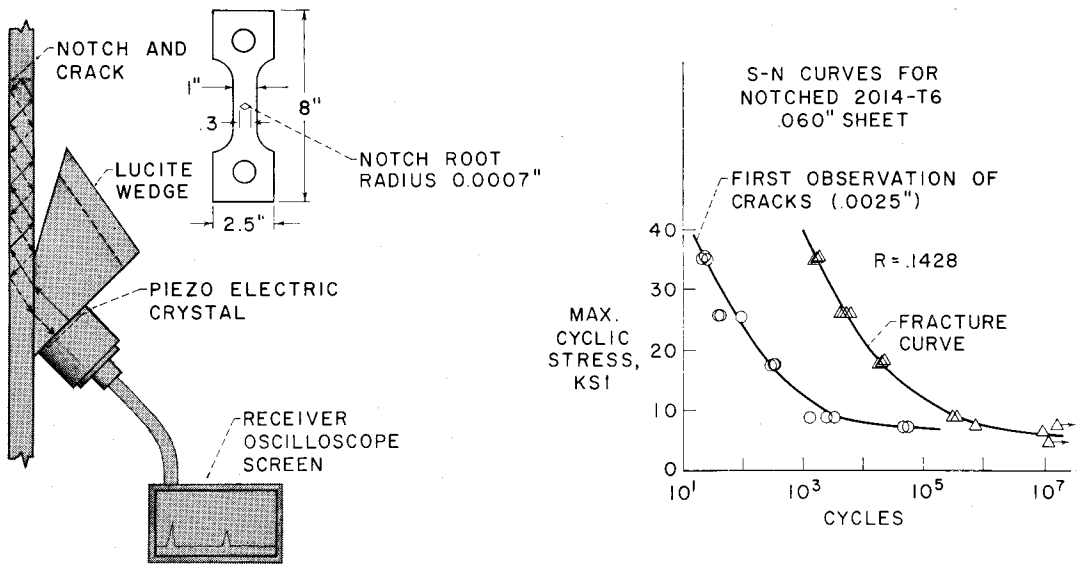

Fig. 14—Ultrasonic technique for detecting early fatigue cracks. (Klima, Lesco and Freche, 1964)

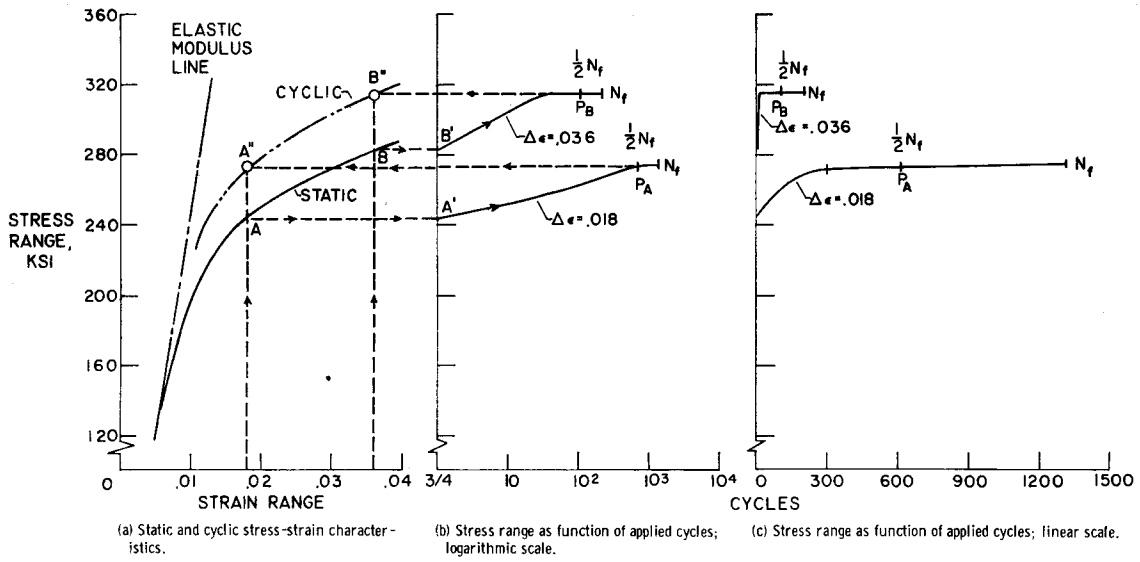

(a) Static and cyclic stress-strain characteristics.

(b) Stress range as function of applied cycles; logarithmic scale.

(c) Stress range as function of applied cycles; linear scale.

Fig. 15—Static and cyclic stress-strain characteristics of 304 stainless steel

reasoning. Within the last 15 years, many new concepts have been generated, and the evaluation of these concepts has produced immense strides in the understanding of the fatigue phenomenon and the application of laboratory data toward control of fatigue failure.

Phenomenological Behavior in Strain Cycling

Although the techniques just outlined for studying the fundamental mechanism of fatigue have produced some very useful results leading to a better understanding of the mechanism, we are as yet far from being able to apply our fundamental understanding to solve the fatigue problem in the field. Practical approaches still involve the direct measurement of fatigue properties of materials. Some of these results may be useful as a first step in design and may also provide some insight into the fatigue mechanism. We shall now discuss some recent results that have been obtained in our laboratory.[14, 15]

Strain-cycling Concepts

Consider a specimen that is subjected to axial reversed strain cycling. First a positive strain $(+\epsilon)$ is applied to the specimen; by reversing the load, a negative strain $(-\epsilon)$ is obtained resulting in a total strain range of 2ϵ. Note that this type of loading is slightly different from what has conventionally been done in fatigue testing wherein the load is the primary variable that is controlled.

The first observation made when a specimen is strained in this manner is that it requires different loads to accomplish a desired amount of strain, depending on the number of prior applications of the strain. This fact is illustrated in Fig. 15. Here, for reference purposes, a continuous curve is plotted to illustrate static stress–strain behavior of the material. The stress is plotted, however, as a *range*, indicating the total range in stress including both the compression and the tension halves of the cycle. Some manipulation is required to transform a conventional stress–strain curve to one involving stress range and strain range, but it is essentially the stress–strain curve of the material. In the first cycle of loading, the stress range required to produce a fixed strain range, for example 0.018, is at point A in Fig. 15(a). It lies on the static stress–strain curve, because, by definition, the static stress–strain curve provides the stress required to produce a given strain in the first quarter cycle of loading. However, if an attempt is made to apply the same strain in successive cycles, it takes a greater stress range to maintain the strain range. This fact is illustrated in Fig. 15(b) along the line $A'P_A$. In this case, after about 600 cycles of loading, however, the stress stabilizes and for the remainder of the test, out to about 1400 cycles, the stress range remains approximately constant. This achievement of an asymptotic stress range is sometimes referred to as "saturation hardening." If the asymptotic stress range that is reached is plotted against the applied strain range, this point falls on A'' in Fig. 15(a). In a similar manner, if the strain range is raised to 0.036, the variation $B'P_B$ is obtained, resulting in the point B'' in Fig. 15(a) as the asymptotic stress range associated with the strain range 0.036. The curve joining A'' and B'' represents what is known as the "cyclic stress–strain curve." In this case, it lies considerably above the static stress–strain curve; this material is thus referred to as a *cyclic strain-hardening* material. Of additional interest is the plot in Fig. 15(c), which is merely a replot of Fig. 15(b) with the cyclic-life scale made linear. It is apparent from Fig. 15(c) that saturation hardening is achieved during the early cycles of loading, usually well before half the number of cycles to failure have been applied.

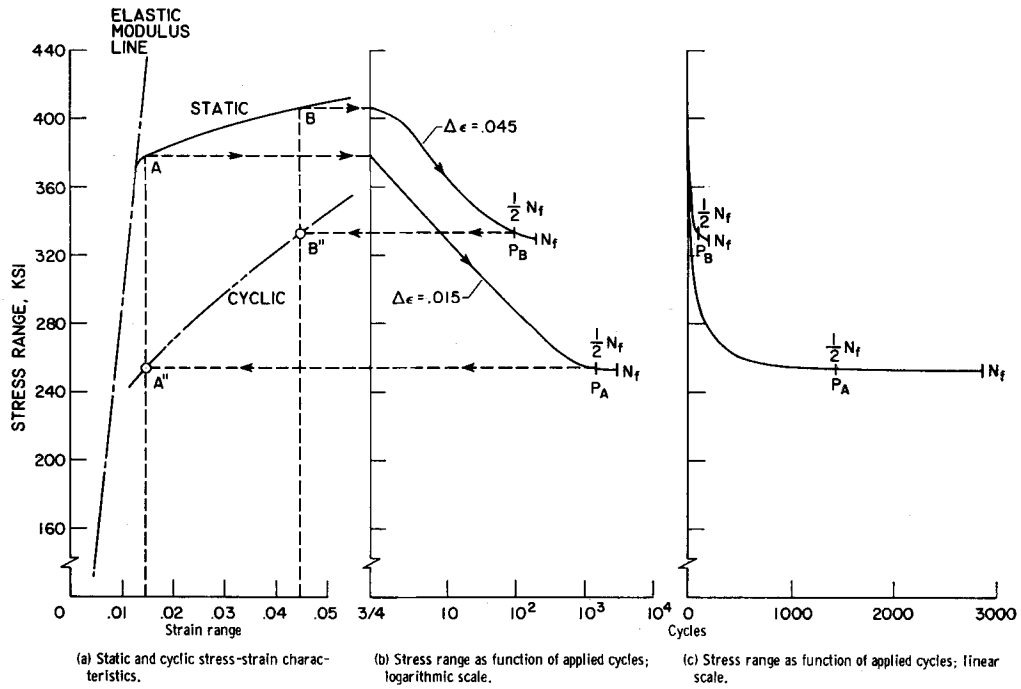

Fig. 16—Static and cyclic stress–strain characteristics of 4340 steel

Figure 16 illustrates the behavior of another class of material described as *cyclic strain softening*. In this case, for a strain range of 0.015, the stress range required is initially at point A, but it quickly diminishes until, after a relatively few cycles, the stress range is only about half that at point A. The cyclic stress–strain curve here is $A''B''$ and falls considerably below the static stress–strain curve. The degree of hardening or softening varies considerably among materials, and some materials even show hardening and softening in the same test.

Before presenting an analysis of the data, it is important to discuss some details of procedure used in our investigations. Some of the conflicting reports that have appeared in the literature regarding strain–cycling data are due in part to a lack of clear description of the procedure that is followed in obtaining the data.

As already indicated, the tests referred to here[15] are for strain cycling about zero mean strain. In most of these tests, the transverse strain range (diametral) rather than the axial strain range was maintained constant. This was done in order to produce known values of true strain in the region where failure occurs. A specimen of hourglass shape was found most convenient for these tests. When analyzing the data, the life was taken as the number of cycles required to cause complete rupture of the specimen. It is important to make a distinction here because some investigators regard the life of a specimen as the point at which cracks begin to appear on the surface. Later the difference between these two concepts will be interpreted.

When saturation hardening or softening actually occurs, the value of stress range in the cyclic stress–

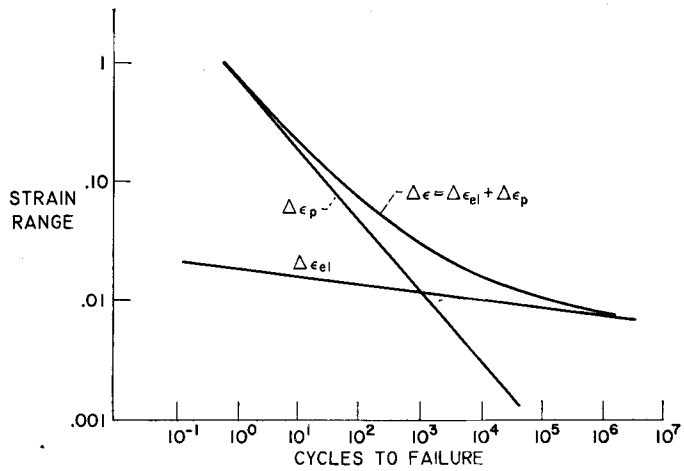

Fig. 17—Total strain as combination of two linear relations

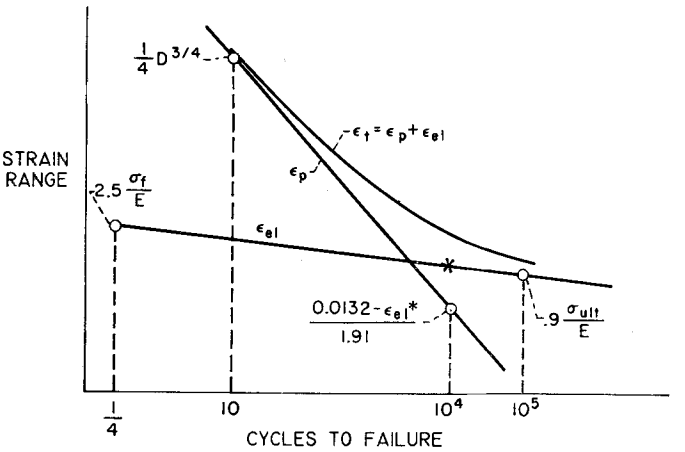

Fig. 18—Method of predicting axial fatigue life based on ductility, fracture strength and ultimate strength

strain curve is unambiguous. In some cases, where hardening or softening continues throughout the test, the value of stress range used is that at the half-life of the specimen.

When a total strain range $\Delta\epsilon$ ($= 2\epsilon$) is applied to a specimen (in our tests the axial strain range is deduced from a knowledge of stress range, diametral strain range and the elastic constants), that part of the total strain range, which is elastic, can be separated from that which is plastic by a knowledge of the stress range. The elastic strain range is simply the stress range divided by the elastic modulus. The plastic strain range is obtained by subtracting the elastic strain range from the total strain range. Figure 17 shows idealized results that are obtained when fatigue life is plotted against either the elastic or plastic strain range. Straight lines result when both scales are logarithmic. The curve depicting the total strain range, which is the sum of these two components, is also shown in the figure.

The concept that cyclic life is related to the plastic strain range was first proposed by us in 1952.[16] This resulted from our effort to estimate the importance of temperature on the thermal-stress fatigue of turbine buckets. Since then, a considerable number of studies have been made by many investigators to verify the relation. The linearity of elastic range with life has been proposed more recently[17] in an effort to overcome the difficulty, from a practical point of view, of determining life from the plastic range only. It is usually the total strain that is known rather than the plastic strain, and therefore it is difficult to estimate how much of this strain is plastic until the elastic component is known. For this reason, it is much more useful, in practice, to relate life to the total strain, which is the sum of the elastic and plastic components.

It will be noted that the total strain range is not a straight line. Because of the logarithmic scale involved, the curve of total strain range against life is asymptotic to the plastic line in the lower cyclic-life range, and the elastic line in the higher cyclic-life range.

Prediction of Axial Fatigue Life from Tensile Data

From a practical point of view, merely knowing that the elastic and plastic components are approximately straight lines is extremely useful because it means that only a few tests are needed to establish these lines. There are, however, many applications when it is desirable to avoid any fatigue testing whatsoever and to estimate these straight lines from a knowledge of more readily obtained material properties. Therefore, an attempt has been made to establish a correlation between these lines and the properties of materials obtained in simple tensile tests.

FOUR-POINT-CORRELATION METHOD—Figure 18 shows one method of analysis that we have investigated. It may be referred to as a four-point method because the two straight lines are obtained by locating two points on each of them. Every point is determined from a knowledge of the tensile behavior of the material. A point is located on the elastic line at $^1/_4$ cycle with an ordinate $(2.5\ \sigma_f)/E$, where σ_f is the true fracture stress of the material obtained by dividing the load at the time of failure in the tensile test by the actual area measured after failure has occurred. Another point on this line is obtained at 10^5 cycles. At this point, the ordinate is $(0.9\ \sigma_u)/E$, where σ_u is the conventional ultimate tensile strength of the material. On the plastic line, a point at 10 cycles is determined that has an ordinate of $^1/_4D^3/_4$, where D is the logarithmic ductility of the material defined as the natural logarithm of the original cross-sectional area of the specimen divided by the final cross-sectional area. The second point on the plastic line is obtained at 10^4 cycles as indicated in Fig. 18. The point shown by the star at 10^4 cycles is first located on the elastic line and the ordinate observed. This ordinate is then substituted into the simple equation shown in the figure to obtain a corresponding ordinate value at 10^4 cycles for the plastic strain. This formula is derived from the observation that the plastic and the elastic strains at 10^4 cycles are approximately related to each other. The relation is almost (but not quite, see Ref. 15) equivalent to the assumption that the total strain range at 10^4 cycles is approximately 1 percent for all materials. Thus, from a knowledge of the tensile properties, two points on each of the lines can be determined and the plastic and elastic components plotted as in Fig. 18. The curve of total strain range may be obtained by simple addition, as indicated by the curved line, which is asymptotic to the plastic line in the low-life range and to the elastic line in the high-life range. This curved line thus represents the estimated relation between total strain range and life for the material.

In order to obtain the fatigue properties in this way, the true fracture stress must be known; however, this property is not always given in the literature, and therefore an additional approximation is sometimes required. A very good approximation has been suggested by John O'Brien* who, under contract with NASA, recommended that the fracture stress could be obtained by multiplying the ultimate tensile strength by the factor $(1 + D)$. Thus,

$$\sigma_f = \sigma_u(1 + D) \qquad (1)$$

That this relation is valid is seen in Fig. 19, where fracture stress is plotted against the product of $\sigma_u(1 + D)$ Each data point represents a different material, and the data generally fall close to a 45-deg line. By using this approximation, only the elastic modulus and two tensile properties, σ_u and reduction in area (which establishes D), are needed to predict axial fatigue life for a specified strain range. This is illustrated in Fig. 20. One simply

* *San Diego, Calif.*

locates the value of σ_u/E and the value of percent reduction in area on the horizontal axis, and then determines the intercepts at P_1 and P_4 from the dashed and solid families of curves. The location of points P_2 and P_3 are obtained from the auxiliary vertical and horizontal scales in the figure.

The procedure described for determining the elastic and plastic lines was first developed by study of relatively few materials. Subsequently, the validity of this procedure was investigated by examining a larger number of materials. Those materials that have been studied in axial low-cycle fatigue tests to date are shown in Table 1. Alloys of nearly all the important classes of structural materials are included.

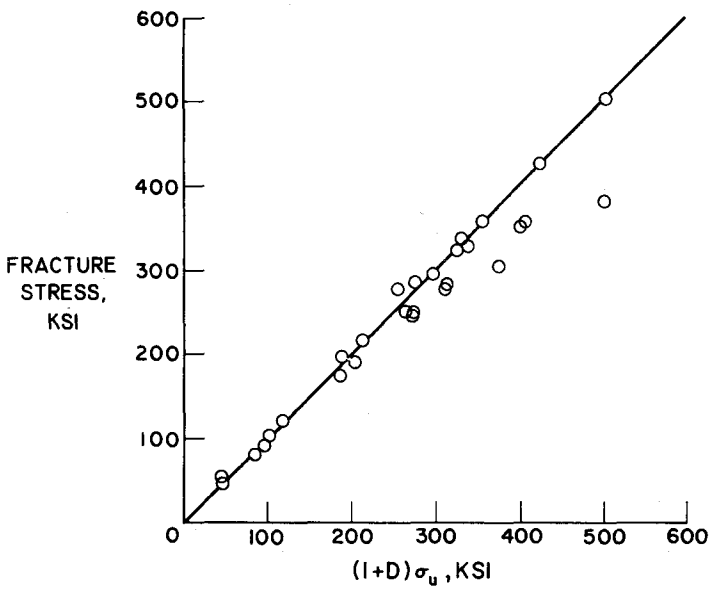

Fig. 19—Fracture stress against function of true ductility and ultimate strength

TABLE 1—MATERIALS FOR AXIAL LOW-FATIGUE INVESTIGATION

4130 Soft	Titanium 6A1-4V
4130 Hard	Titanium 5A1-2.5Sn
4130 X-hard	Magnesium AZ31B-F
4340 Annealed	Aluminum 1100
4340 Hard	Aluminum 5456 H311
304 Annealed	Aluminum 2014 T6
304 Hard	Aluminum 2024 T4
52100 Hard	Aluminum 7075 T6
52100 X-hard	Silver 0.99995 pure
AM 350 Annealed	Beryllium
AM 350 Hard	Inconel X
310 Stainless	A286 aged
Vascomax 300 CVM	A286 34 percent cold reduced and aged
Vascojet MA	D979
Vascojet 1000	

These materials cover quite a range in variables that might affect fatigue behavior such as those shown in Table 2. Among them are crystalline structures wherein body-centered-cubic, face-centered-cubic, and hexagonal-close-packed arrangements are represented; reductions in area covering the range from 1 to 94 percent; tensile strengths from 16,000 to over 400,000 psi; high and low notch sensitivities; cyclic-hardening and -softening characteristics; high and low stacking-fault energy; etc. Thus, any conclusion that might be reached regarding the validity of the relations involving all of these materials cannot be regarded as being limited to a very small class of materials.

METHOD OF UNIVERSAL SLOPES—An alternate approach is to assume that the slopes of the elastic and plastic lines are the same for all materials. In Ref. 17, the universal slope for the plastic line was assumed to be -0.5 and for the elastic line -0.12.

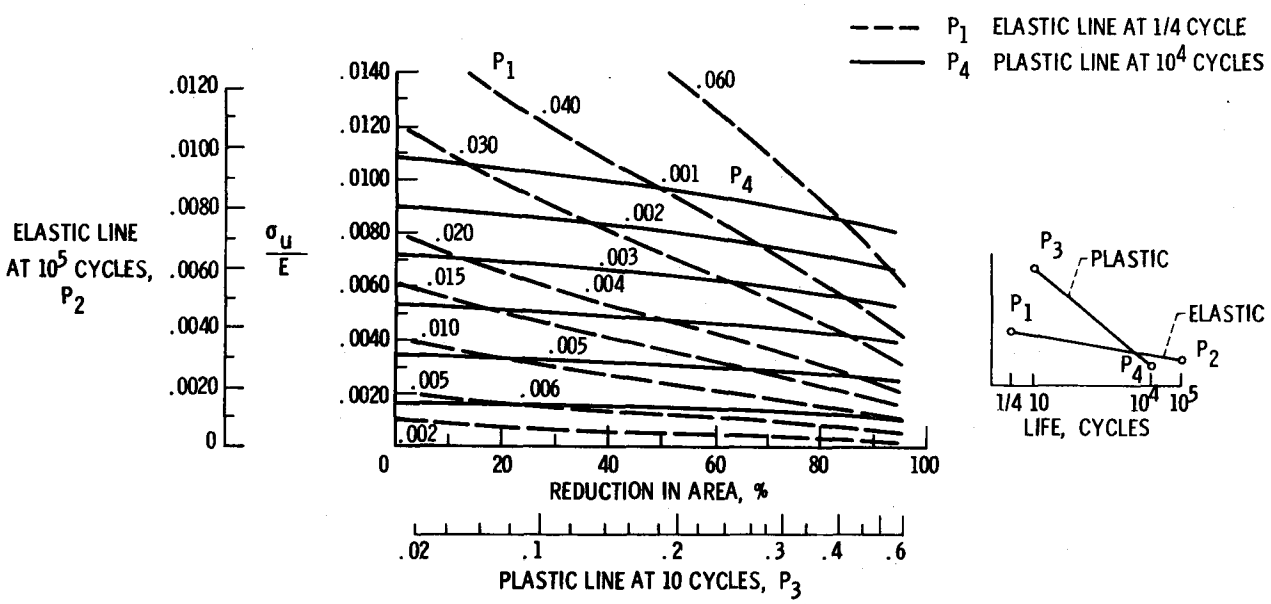

Fig. 20—Predicting axial fatigue from tensile data by four-point-correlation method

TABLE 2—MATERIAL VARIABLES IN AXIAL LOW-CYCLE FATIGUE INVESTIGATION

Crystalline structure	Body-centered cubic Face-centered cubic Close-packed hexagonal
Methods of strengthening	Precipitation hardening Hot and cold worked
Reduction in area	1 to 94 percent
Tensile strength	16,000 to 411,000 psi
True fracture stress	48,000 to 500,000 psi
Elastic modulus	6.2×10^6 to 42.0×10^6 psi
Notch sensitivity	Notch ductile to very notch sensitive
Stacking-fault energy	Low (steels) to high (aluminum)
Cyclic behavior	Strain softening to strain hardening

Data obtained more recently have permitted the selection of more refined values, as indicated in Figs. 21 and 22. Here the results of tests on 29 materials are shown. For the plastic line (Fig. 21), all the data can be represented reasonably well by a straight line with a slope of -0.6. For the elastic line, all the data can be represented reasonably well by a single straight line of slope -0.12. The lines of Figs. 21 and 22 also permit the determination of a single point through which the lines of the known slopes may be drawn. Thus, letting $N_f = 1$ in each of the equations in the two figures, shows the intercept of the plastic line at $N_f = 1$ to be $D^{0.6}$, and the intercept of the elastic line to be $3.5\ \sigma_u/E$. The basic construction of the lines of universal slope is shown in Fig. 23, where it is indicated that, starting at $N_f = 1$ and ordinates of $D^{0.6}$ and $3.5\sigma_u/E$, respectively, for the plastic and elastic lines, these lines are then completed by drawing slopes of -0.6 and -0.12, respectively. The equation for total strain range $\Delta\epsilon$ then becomes

$$\Delta\epsilon = 3.5\,\frac{\sigma_u}{E}\,N_f^{-0.12} + D^{0.6}N_f^{-0.6} \qquad (2)$$

where

σ_u = ultimate tensile strength, psi
D = ductility, $\ln \frac{1}{1 - RA}$
RA = reduction in area, percent
N_f = number of cycles to failure

Figure 24 provides an additional aid to the construction of the elastic and plastic lines based on

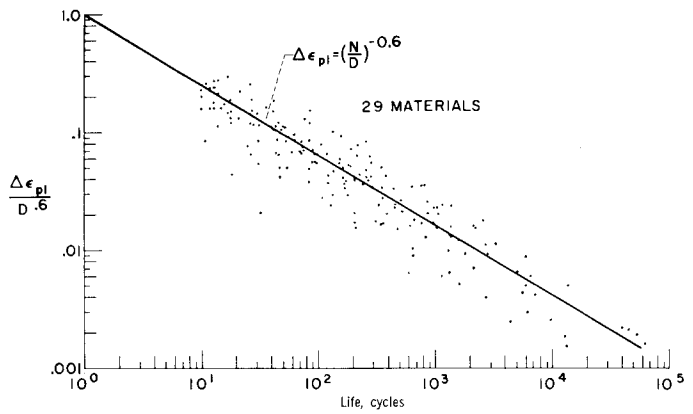

Fig. 21—Relation between plastic-strain ductility and cycles to failure

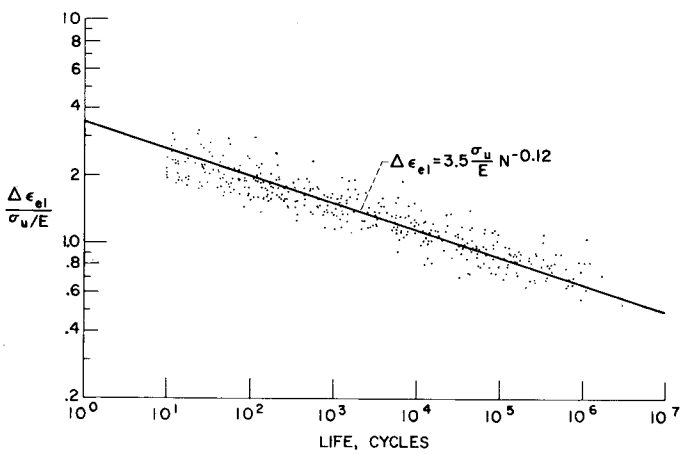

Fig. 22—Ratio of elastic strain range to σ_u/E against cycles to failure (29 materials)

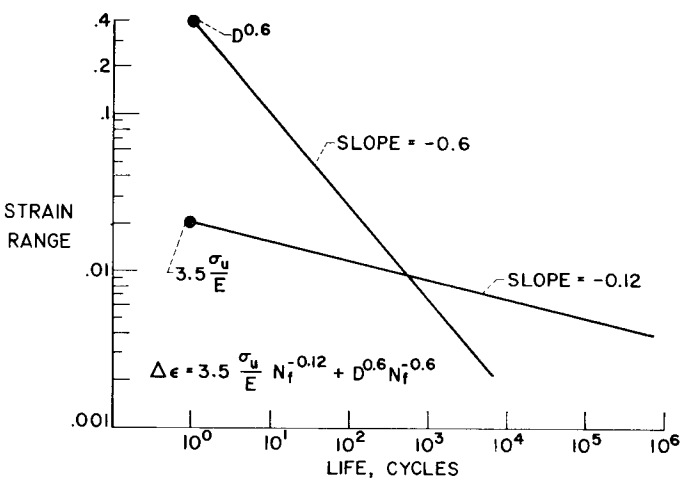

Fig. 23—Model for method of universal slopes

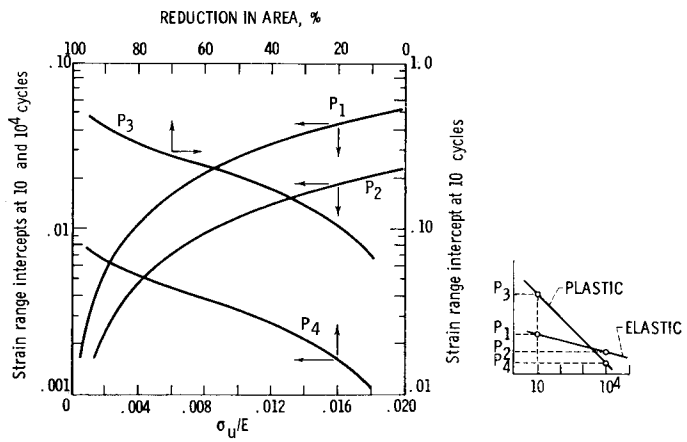

Fig. 24—Predicting axial fatigue from tensile data by method of universal slopes

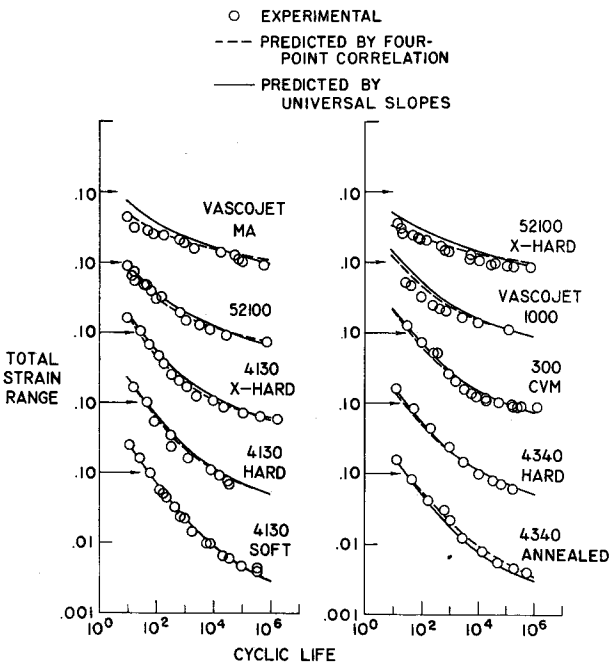

Fig. 25—Comparison of predicted and experimental axial fatigue life for low-alloy and high-strength steels

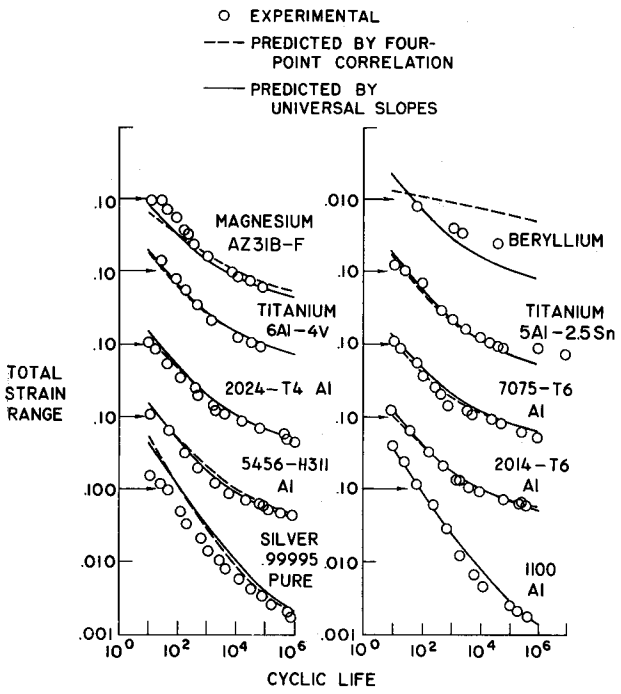

Fig. 27—Comparison of predicted and experimental axial fatigue life for nonferrous metals

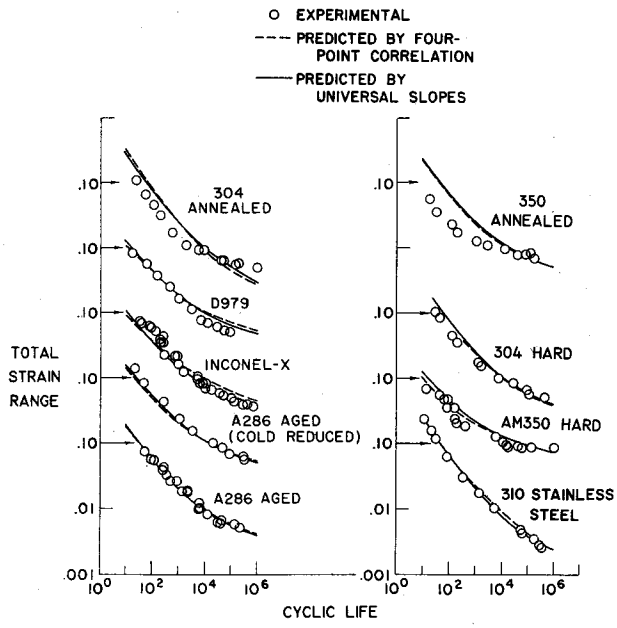

Fig. 26—Comparison of predicted and experimental axial fatigue life for stainless steels and high-temperature alloys

eq (2) using two points on each line (at 10 and at 10^4 cycles). The identification of points P_1 to P_4 and the determination of the ordinates from a knowledge of only RA and σ_u/E may be obtained from the figure. The arrows on each curve indicate the appropriate scales to be used.

Comparison of Prediction Methods

Figures 25 to 27 present the actual comparisons between the experiments and the predictions for each of the 29 materials tested when analyzed on the basis of each of the methods indicated. The individual data points for total strain range (i.e., the sum of the elastic and plastic components) are shown as circles. The predictions by the four-point correlation (including the knowledge of the fracture stress) are shown by the dashed lines. Predictions based on the method of universal slopes are shown by the solid lines. In most cases, the agreement is remarkably good. For AM 350 annealed (Fig. 26) and beryllium (Fig. 27), the agreement is not as satisfactory.

An over-all evaluation of the four-point method is shown in Fig. 28. Here the measured life for each of the test points is plotted against the predicted life from a knowledge of the fracture stress, ultimate tensile strength and ductility. The relation between the data points and the line is indicated by the table at the lower right. Thirty-five percent of the data points fall within a factor of 1.5 in life from the predicted value. Almost 90 percent fall within a life factor of 5. Since some scatter in life is expected in fatigue data, it can be seen that this correlation must be regarded as satisfactory. A few data points, notably those associated with poorly behaved materials like beryllium, are fairly remote from the correlation line, thus resulting in the conclusion indicated by the table that, with an allowable error of a factor of 20 in life, only 97 percent of the data points will

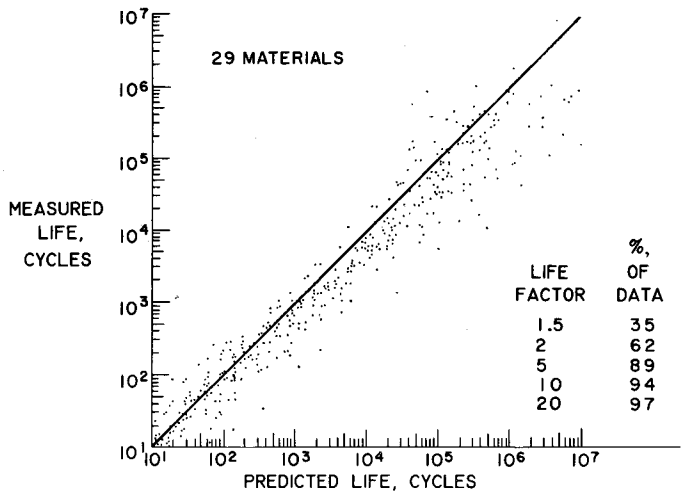

Fig. 28—Measured fatigue life as function of predicted life determined by four-point correlation

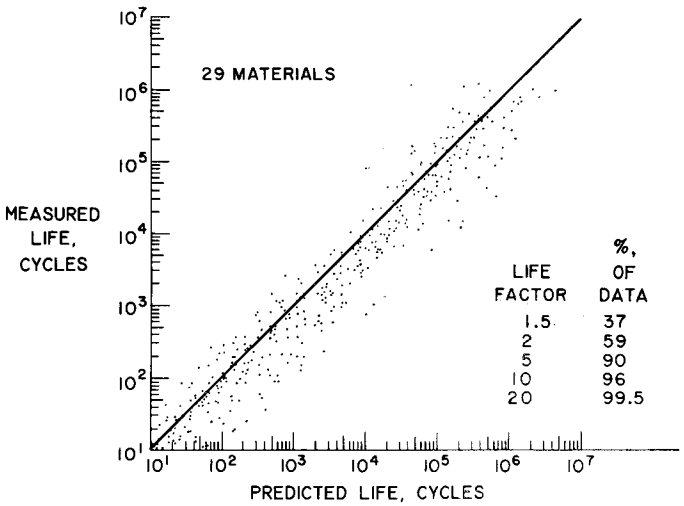

Fig. 30—Measured fatigue life as function of predicted life determined by method of universal slopes

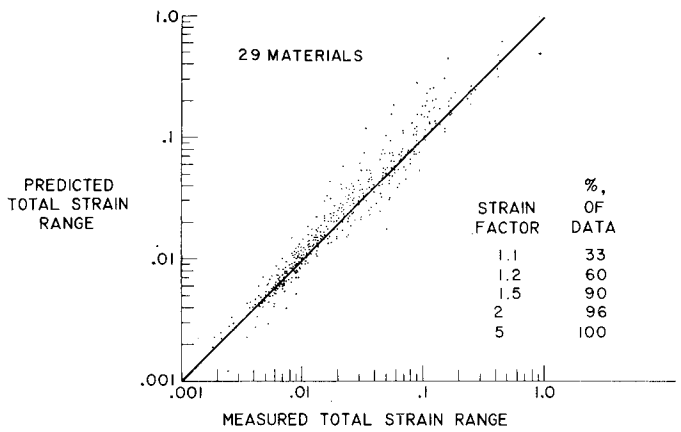

Fig. 29—Predicted strain range as function of measured total strain range by four-point correlation

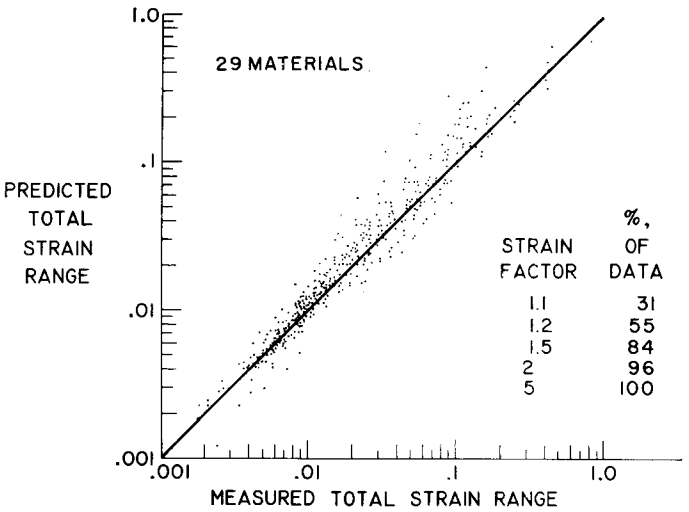

Fig. 31—Predicted strain range as function of measured total strain range by method of universal slopes

be satisfactory. Similarly, Fig. 29 compares the data on the basis of measured and predicted strain range rather than on the basis of life. The total strain range predicted to produce the life observed in each test is plotted on the ordinate. The measured total strain range is plotted on the abscissa. The correlation is, as might be expected, considerably better. Ninety percent of the data points fall within a strain factor of 1.5.

Figure 30 shows a corresponding over-all comparison on a life basis for the method of universal slopes. Similarly, Fig. 31 shows the comparison on the basis of predicted strain for the same 29 materials as obtained by the method of universal slopes. The agreement with experiment is, in both cases, approximately the same as that obtained by the four-point method.

Alternate Relation for Predicting Axial Fatigue Life in Terms of Endurance Limit

In the preceding discussions, strain has been expressed in terms of the elastic and plastic components, both of which were linear when plotted against life on log-log coordinates. This approximation is extremely useful in practical applications. When one attempts to express life directly in terms of strain, however, the resulting equation does not readily lend itself to a closed-form expression. There is also another minor objection to the manner of relating strain and life thus far discussed. This is the fact that it does not provide for the possibility of the existence of an endurance limit strain, a strain below which the life is essentially infinite. Figure 32 indicates an alternate relation, which, in a sense, overcomes

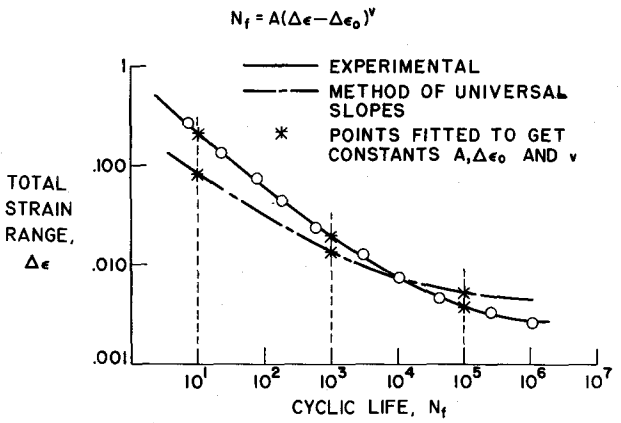

Fig. 32—Alternate equation for life in terms of total strain range

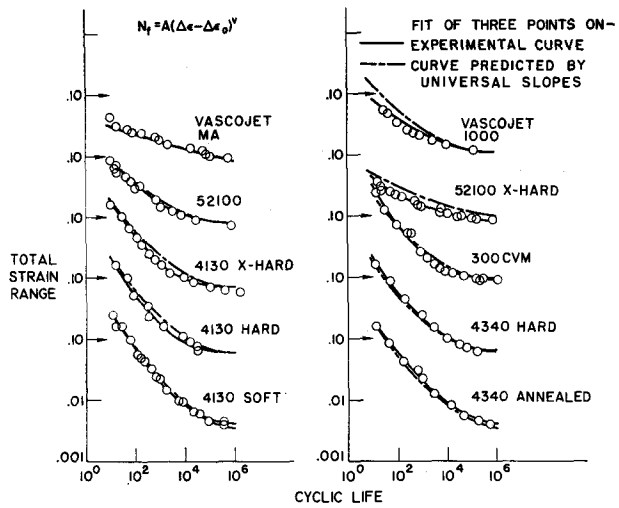

Fig. 33—Comparison of predicted and experimental axial fatigue life for low-alloy and high-strength steels using alternate equation involving endurance limit

both of these objections. Cyclic life N_f is expressed in terms of the applied total strain range $\Delta\epsilon$, without regard to what percentage is elastic or plastic. This equation is

$$N_f = A(\Delta\epsilon - \Delta\epsilon_0)^v \qquad (3)$$

Included in the operation is a constant, $\Delta\epsilon_0$, which is an endurance-limit strain. Below $\Delta\epsilon_0$, life is taken as infinite. This expression will obviously coincide with the plastic strain equation when $\Delta\epsilon$ is large, as is the case in the very low-cyclic-life range. That is, for large values of $\Delta\epsilon$ the value of $\Delta\epsilon_0$ becomes negligible, and a power-law relation between life and plastic strain results. Thus, the term A would be expected to be of the order of the coefficient in the plastic strain relation and v to be of the order of the exponent of the plastic-strain relation.

For the purpose of determining whether a relation of the type shown in Fig. 32 is valid for the 29 materials, an attempt was made to determine the three constants A, $\Delta\epsilon_0$ and v by satisfying the equation at three points: cyclic lives of 10, 1000 and

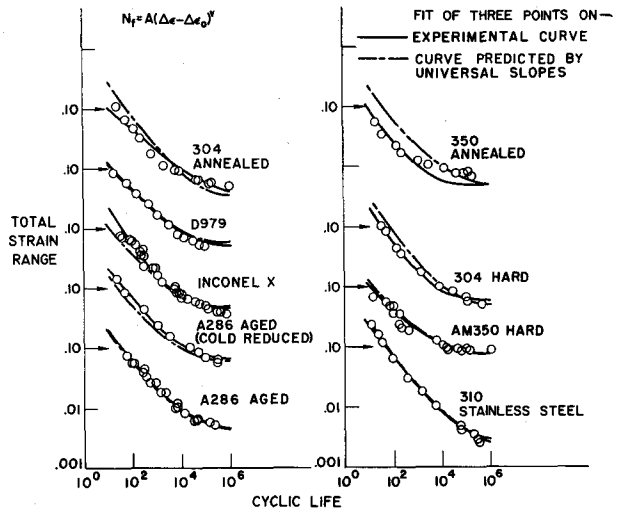

Fig. 34—Comparison of predicted and experimental axial fatigue life for stainless steels and high-temperature alloys using alternate equation involving endurance limit

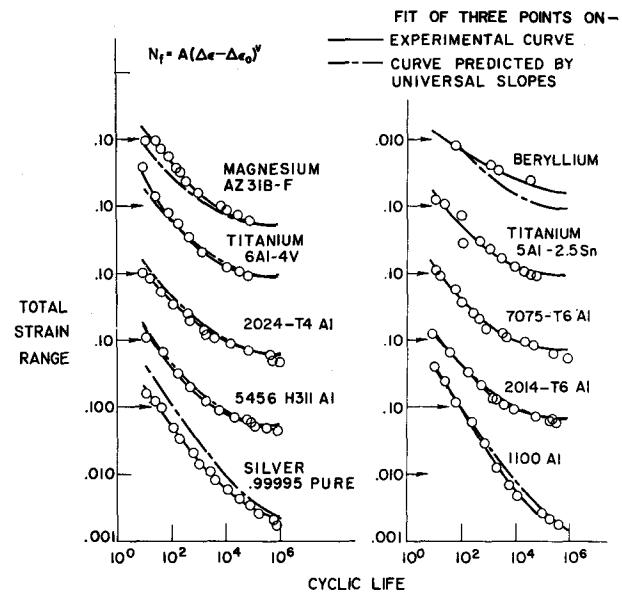

Fig. 35—Comparison of predicted and experimental axial fatigue life for nonferrous metals using alternate equation involving endurance limit

100,000 cycles. One approach involved the selection of three points on the experimental curve determined from actual data. In a second approach, three points were selected from the curve predicted by the method of universal slopes and the constants subsequently obtained. Both these methods are illustrated in Fig. 32. The degree of discrepancy shown in this figure between the experimental data and the curve of universal slopes has been emphasized for the sake of clarity. Figures 33 to 35 show the actual comparison between the experimental and predicted curves for all 29 materials by using eq (3).

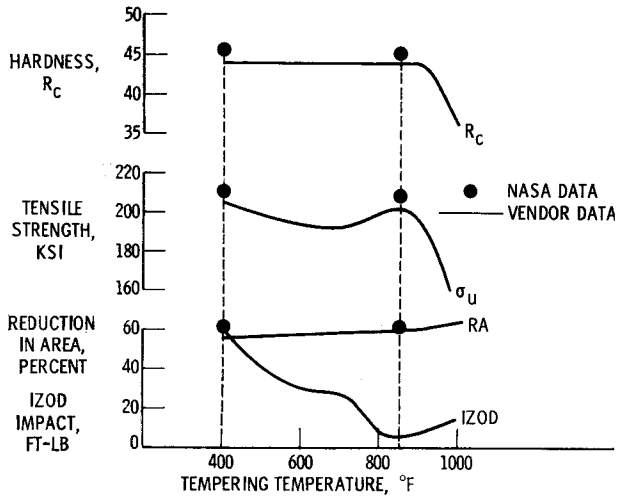

Fig. 36—Mechanical properties of Type 410 stainless steel quenched from 1850° F

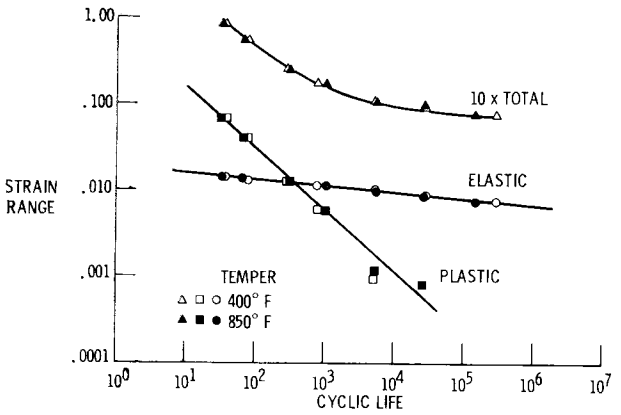

Fig. 37—Axial strain-cycling fatigue of 410 stainless steel in two conditions of temper

Since the strain values at the lives indicated by the stars on the dot-dash curve (Fig. 32) can be expressed explicitly in terms of ductility and ultimate strength, it is apparent that A, $\Delta\epsilon_0$ and v can also be determined explicitly in terms of these two simple measurable properties. The algebraic relations that result, however, are quite complicated and will not be described here. The important point to be made is illustrated in Figs. 33 to 35. In these figures, the solid lines illustrate the agreement between the data and the curves obtained by means of the equation shown at the top of the figures when the constants are determined from a knowledge of the experimental data at three values of life. The dash–dot curves provide a similar comparison when the constants were determined from curves drawn by the method of universal slopes. Obviously, corresponding curves could be drawn to represent the points as predicted by the four-point approximation method. In each case, the fit coincides almost exactly with the corresponding fit associated with the method of universal slopes and is, therefore, not shown. The main feature that is demonstrated is that the equation for life in terms of strain range can be represented by an equation of the type shown in eq (3) and that, where appropriate, this equation may be used instead of the ones discussed previously.

Effect of Yield Stress and Notch Sensitivity on Fatigue Life in Strain Cycling

The previous discussion emphasized the importance of ultimate tensile strength and reduction in area as principal variables governing strain-cycling fatigue behavior. Before drawing any final conclusions, however, it is important to consider the possible significance of other properties—for example, yield stress and notch sensitivity. That yield stress cannot be a property of primary influence on the fatigue characteristics can be seen from Figs. 15 and 16, which have already been discussed in connection with the cyclic stress–strain relation. Since only a very few cycles can drastically change the stress required to produce a given strain, it can be seen that the initial yield stress is of little meaning in the major number of cycles within a given fatigue test. The yield stress as determined in a virgin material can thus be dismissed as a property of primary importance in governing fatigue life in the low-cycle range.

The second variable, notch sensitivity, requires more extensive consideration before its proper role can be assessed. That materials vary appreciably in their notch characteristics, and that notch sensitivity is classically linked to fatigue resistance are well established. Since this property has not entered into the correlation thus far discussed, it is desirable to question the appropriateness of the omission, and if appropriate, then why?

In order to ascertain whether the fatigue results are affected by notch sensitivity, a series of tests was conducted in which the same material was heat treated to achieve different degrees of notch sensitivity while maintaining the same tensile strength and ductility. The basis of the tests is indicated in Fig. 36. Here published data for stainless steel 410 are shown. The center curve shows tensile strength as a function of tempering temperature. It can be seen that tempering at either 400° or 850° F produces approximately the same tensile strength. Correspondingly, the reductions in area for these two heat treatments are almost identical. The impact resistance as indicated by the lowest curve, however, is very seriously affected by the tempering temperature. Tempering at 850° F produces a material of much lower impact resistance than the one tempered at 400° F. From this it might be inferred that the 850° F temper produces a notch-sensitive material. We have conducted notch tests on sheet at our laboratory with this steel that verified this conclusion. The 850° F temper was extremely notch sensitive. As a result, we had the opportunity of testing two materials with identical tensile strengths and ductility but far-different notch-sensitivity values.

The axial strain-cycling fatigue behavior of this material in these two conditions of temper is shown in Fig. 37. Open data points refer to the 400° F temper and closed data points refer to the 850° F temper condition. Although there is a small amount of scatter, it can be seen that the two materials produced approximately the same fatigue resistance; there was quite a difference in the appearance of the fracture surface, however. The 850° F tempered material frequently showed very brittle fracture surfaces, while in many cases the 400° F tempered material showed very ductile fracture surfaces. Nevertheless, as far as cyclic life is concerned, the two results were quite similar.

In order to understand these results, it is necessary to undertake consideration of crack occurrence in a fatigue test of the kind that is being considered here. In our laboratory, we have attempted to observe the initiation of a crack by several methods. One of the more interesting approaches has been by the use of a polycarbonate resin material. Admittedly, because this material is a plastic, it does not quite fit in with the fatigue analysis that has been presented. Nevertheless, it has been quite useful in gaining an understanding of crack growth. We shall first present the data obtained with this material because it has a visual attractiveness. At the same time, it should be recognized that the conclusions drawn will not be inconsistent with the behavior of metallic materials. Figure 5 has already been used to show why polycarbonate materials are so useful in the study of crack growth. Striations are clearly evident on the fracture surface on a macroscopic scale. Each cycle is clearly delineated and can readily be determined. The particular specimen of Fig. 5 had a life of 115 cycles. By counting back from the last cycle, it is possible to determine exactly where crack growth stopped at each cycle of loading. Figure 38 shows the analysis of the data for this specimen and for one which had a life of 1300 cycles. The crack depth is plotted against percent of fatigue life. The limit of resolution of these cracks was of the order of a depth of 0.002 to 0.003 in. It is clear from this figure, however, that a crack depth of the order of this magnitude starts quite late in the life of the specimen, approximately 65 percent of the life for the low-cycle test and 85 percent for the high-cycle test. Figure 39 provides a summary of the results of a number of tests conducted to determine approximately when, in the life of an axially cycled specimen, the crack reaches a size of 0.002 to 0.003 in. Several types of data are shown in this figure. The data represented by open circles are taken from Laird and Smith.[18] They obtained their results by counting striations on specimens of pure aluminum and nickel. The closed circles represent the polycarbonate data already discussed. The triangles represent data obtained at our laboratory with 2024-T4 aluminum from surface observations. The data correspond to the percent of total life required to produce surface-crack lengths of the order of 0.010 in., which were visible without magnification. Also shown are results for 4130 steel and 410 stainless steel. These data were also obtained from surface observations. For later use, it will be desirable to express the data in Fig. 39 by an analytical expression. A plot of $1 - (N_0/N_f)$ against N_f on log-log coordinates results in a straight line defined by the equation

$$1 - (N_0/N_f) = 2.5\, N_f^{-1/3} \qquad (4)$$

where

N_0 = number of cycles to visible cracking.
N_f = number of cycles to complete fracture.

This equation is obviously only approximate, and at best is valid only for values of N_f higher than 15 cycles. For values of N_f below 15 cycles, the equations would imply that N_0/N_f is negative. Equation (4) is plotted in Fig. 39 and is seen to fit the data quite well, although data are, of course,

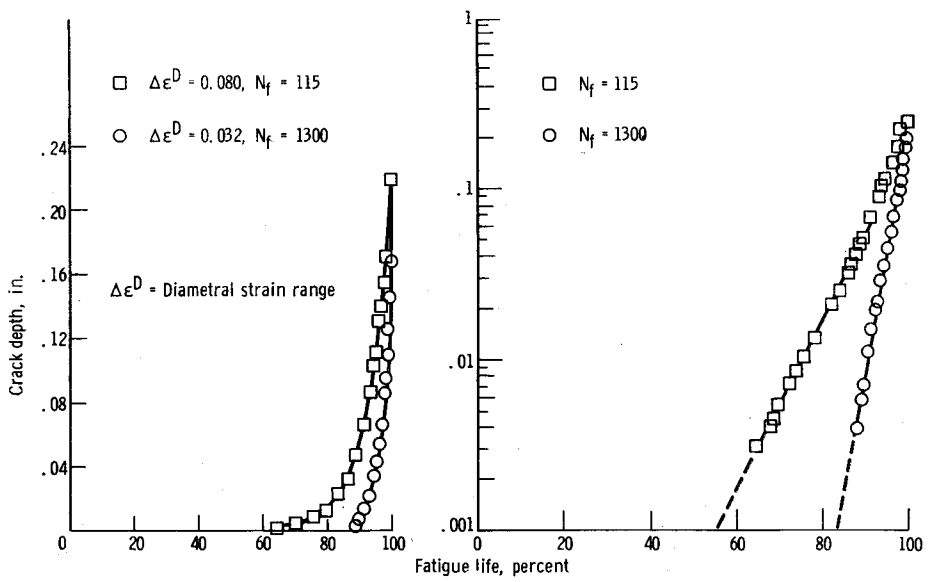

Fig. 38—Crack-growth curves for polycarbonate resin

(a) Rectangular coordinates. (b) Semilogarithmic coordinates.

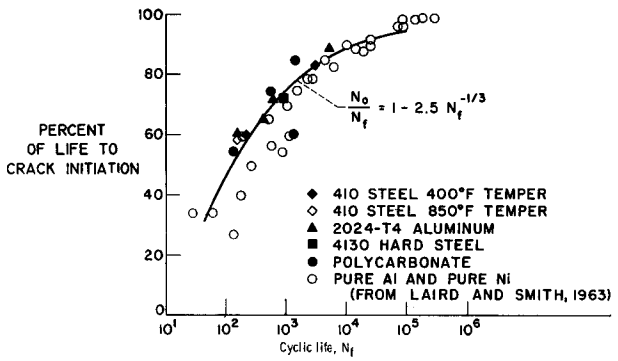

Fig. 39—Relation between percent of life to crack initiation and fatigue life

inadequate to ensure that all materials can be represented by a single curve. Probably a series of curves dependent upon crack size chosen, and to some extent on grain size and notch toughness of the materials should be expected. An important point to be observed from this curve is that only for the very low cyclic-life tests does a crack of any appreciable size occur early in the life of a specimen. For cyclic lives for the order of 1000 or more, detectable cracking does not occur until nearly 70 percent or more of the cyclic life has been used up.

Now it is axiomatic that a material, which is sensitive to notches or cracks, will not manifest its sensitivity until the crack of significant size to alter the stress field actually develops. If such a crack does not occur until quite late in the life of the specimen, the material cannot be sensitive to it until most of the life has already been used up. Since the type of test under consideration here, namely, a small specimen subjected to axial cyclic strain loading, does not involve significant cracking until very late in its life, it might be expected that the behavior of the material in the presence of such a crack will not significantly affect the result. Even if the material were to fail immediately on the development of a small crack, the life would be reduced on the order of 50 percent at a life of 100 cycles, and much less for the higher cyclic lives. Considering normal data scatter, this reduction might be difficult to detect in the analysis of the data. It is concluded, therefore, that the important feature of axial strain cycling tests of unnotched specimens is the very late development of significant cracking and, therefore, that the principal reason why tests of this kind do not reflect notch sensitivity is that cracks of significant size are not present in these materials during the major portion of their life.

One might ask whether these tests are therefore realistic since many component parts are, indeed, operated in the presence of cracks. Furthermore, in many cases, there are large bodies in which crack propagation constitutes a great portion of the life. This question will be touched on later in the section on cumulative fatigue damage. At this point, it is important to recognize that the task we have set for ourselves was to estimate the axial fatigue life of a particular specimen in a particular type of test, one that is frequently used, and the one that was used to obtain the data shown in the previous figures. The problem we set about to discuss was how to estimate the results of these axial fatigue tests from the tensile properties of the materials and whether notch sensitivity should be considered a primary variable. What we have shown is that the answer is negative for the type of specimen employed in the tests, and that the results of these tests can best be estimated by using only the tensile strength and ductility measured on smooth specimens. Whether the results are meaningful in terms of *component operation* is a question equally to be asked of any data obtained on small, unnotched specimens, either by experiment or by estimation by the procedures indicated. The fact that the estimates of fatigue life of small, smooth specimens must be carefully interpreted before they can be applied to estimate the life of a structure is an important consideration that will be discussed later in conjunction with cumulative fatigue damage.

Consideration of Universal Slope for Plastic Strain Line

While we are on the subject of when, during the course of the life of a fatigue specimen, detectable cracking first occurs, it is appropriate to revert to the interesting question of the magnitude of the slope of the plastic strain line. When we first proposed in 1952 that the plastic strain line is linear on log-log coordinates, the proposal was based on very limited experimental data available at that time. Certainly there were not enough data to justify the assumption of a universal slope for all materials. We suggested that the exponent, or slope, would be a material constant. In later investigations, Coffin[19] suggested that the exponent has a universal value of -0.5 for all materials, and for many materials investigated since then, he has concluded the value of -0.5 to be the applicable exponent. On the other hand, the tests that have been conducted in our studies of many materials indicate that the slopes are indeed different from material to material, but that if a universal slope is to be assumed, then a value of -0.6 would be more representative of all materials. It is important, therefore, to reconcile the various observations by different investigators.

Before further discussion of this subject can be undertaken, it is important to consider what is meant by the failure life of a specimen. In some of his tests, Coffin observed the specimen surface, and when visual cracking occurred, he regarded the test complete. Other investigators may also have used initial cracking as the criterion for failure. In all of the tests on the 29 materials in our program, failure was taken as the actual separation of the two halves of the specimen. We can now, there-

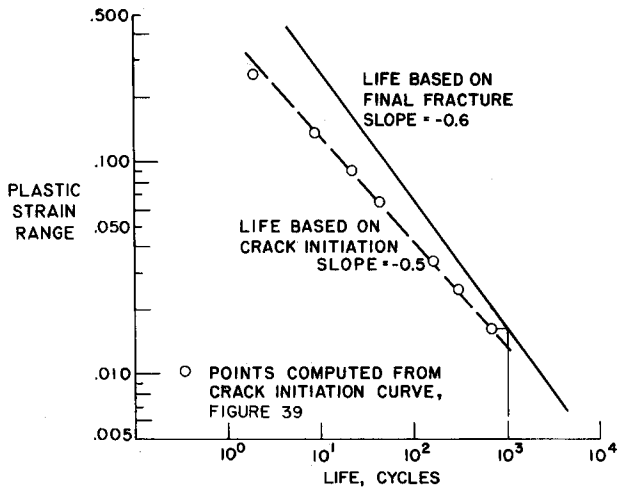

Fig. 40—Relation between plastic strain range and life as determined by crack initiation and by fracture

fore, examine the relation between these two criteria for failure by the use of Fig. 40. This figure illustrates the relation between plastic strain range and life for an idealized material in which the two cases of specimen separation and of cracking are considered. The continuous line shown in this figure is an idealized line, typical of several of the materials investigated showing a slope of −0.6. Since this line presumably constitutes specimen separation, and since we have already indicated in Fig. 39 a relation between cracking and separation, we may now apply the curve of Fig. 39 to estimate when initial cracking might have occurred for this idealized material. Thus, by selecting several life values on the solid line, it may be determined from Fig. 39 when initial cracking probably occurred. These lives are replotted as the circles shown in Fig. 40. It can be seen that, when one passes an approximate straight line through these circles, it has a slope of −0.5. Also of interest is the fact that this straight line can be extrapolated back to an intercept at $^1/_4$ cycle, which is lower than the continuous line. A discrepancy in intercept has also been noted in the literature when cracking is considered as indicative of cyclic life compared with specimen separation. It is not, of course, certain that this is the complete explanation for the discrepancy. Such a wide variation in slopes exists among various materials that many other factors probably contribute to it. Nevertheless, this idealized analysis is interesting and provides some insight as to the possible reason for discrepancies in published results.

Crack Propagation and Its Relation to Power Law for Cyclic Life

Many attempts have been made to explain the power-law relation between plastic strain range (or stress range) and life, but no completely satisfactory rational explanation has as yet been offered. One type of analysis may be made by examining the relation for crack growth. In the following discussion, an attempt will be made to provide a very approximate relation by using a crack-growth concept. It is recognized that this approach is not at all rigorous but may serve as a starting point from which a more valid analysis may be made. At least it points to some of the features required of an analysis of this type in order to be consistent with experimental observations.

We start with an analogy to observations of crack growth in *stress* cycling. It has been observed that the rate of crack growth per cycle in stress cycling is a power law of stress and crack length. Studies of crack growth in reversed *strain* cycling are very limited but, in general, we may observe from the limited information available that the parameter $\Delta\epsilon_p\sqrt{l}$ (where $\Delta\epsilon_p$ is the plastic strain range and l is the crack length) is about as fundamental in strain cycling as $\Delta\sigma\sqrt{l}$ is in stress cycling. Thus, we assume a power-law relation between crack-growth rate and $\Delta\epsilon_p\sqrt{l}$

$$\frac{dl}{dN} = C(\Delta\epsilon_p\sqrt{l})^s \tag{5}$$

where s is a constant as yet to be determined. If the crack-growth rate is directly proportional to $\Delta\epsilon_p$ or to $\sqrt{l}$, then $s = 1$, which will later be seen to be a desirable assumption in order to satisfy the quantitative observations of the plastic power-law exponent.

From eq (5)

$$\frac{dl}{l^{s/2}} = C(\Delta\epsilon_p)^s\, dN \tag{6}$$

Integrating eq (6) between (l_0,N_0) and (l_f,N_f), where l_0 and N_0 are any corresponding values of l and N during which the crack-growth law, eq (6), is valid, and where l_f is the crack length at the cyclic life at fracture N_f, results in

$$\frac{2}{2-s}\left(l_f^{(2-s)/2} - l_0^{(2-s)/2}\right) = C(\Delta\epsilon_p)^s(N_f - N_0)$$
$$= C(\Delta\epsilon_p)^s N_f\left(1 - \frac{N_0}{N_f}\right) \tag{7}$$

The first problem is to select values of l_0 and N_0. As already indicated, these could be *any* corresponding values of l and N during which eq (6) is valid. Frequently (e.g., Ref. 20), this detail is overcome by taking N_0 to be small in comparison with N_f, while l_0 is small compared with l_f; thus, such an analysis proceeds by omitting both the l_0 and N_0 terms in eq (7), resulting in the relation

$$C(\Delta\epsilon_p)^s N_f = \frac{2}{2-s} l_f^{(2-s)/2} \tag{8}$$

By further assuming that the crack length at fracture is approximately constant, the plastic power-law relation follows immediately from eq (8). In fact, if s is taken as 2, we get the universal slope of $-^1/_2$ on a plot of log $\Delta\epsilon_p$ against log N_f, although for a value of $s = 2$, the integration of

eq (6) is not valid as shown since it requires a logarithmic integral of dl/l. This does not change the essential features of the argument, and the same conclusion is reached by treating the equation from the very beginning for $s = 2$ and integrating properly.

While the preceding approach leads to a power-law relation as sought, there are some unsatisfying features associated with it. First, although any set of corresponding values of l_0 and N_0 can be chosen as constants of integration, it must be ensured that these values apply within the range in which the crack-growth law [eq (5)] is valid. The question then develops into one of establishing whether this relation is indeed valid in the very early stages of cycling when the crack is too small to be detected and is perhaps confined to individual grains within an initially smooth specimen. For, if the crack-growth equation is not valid in these early stages, N_0 cannot be taken as negligible in comparison with N_f within the range of validity of eq (5).

To avoid this complication, a refinement is introduced whereby we choose, instead, the values of N_0 and l_0 corresponding to the life at which ripples or striations are already well established on the fracture surface, or at which visible surface cracking can be observed. Then, we can be reasonably certain that the specimen is in the crack-growth stage for which eq (5) was assumed to be valid, while at the same time *not denying* that eq (5) could possibly have been valid at an earlier stage of the life. Choosing such a small value of l_0 permits us to omit the l_0 term on the left side of eq (7), compared with the l_f term (provided that $s < 2$; if $s > 2$ it might, in fact, be permissible to omit the l_f term). We cannot, however, neglect the N_0 term on the right side of the equation. Since we have already determined, in eq (4), the value of $1 - (N_0/N_f)$ as $2.5\ N_f^{-1/3}$, we may substitute this value in eq (7), leaving us with the expression $2.5C(\Delta\epsilon_p)^s N_f^{2/3}$ on the right side of eq (7).

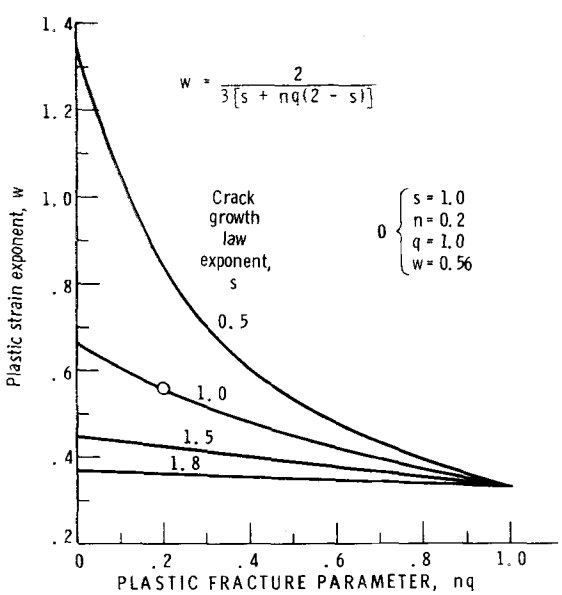

Fig. 41—Relation between plastic-strain exponent and other constants entering into crack-growth and failure laws

A second refinement is to consider the crack length at fracture. In the consideration of brittle materials, the Griffith equation $\Delta\sigma\sqrt{l} = \text{constant}$ has been amply verified. How this equation is to be modified for a ductile material in strain cycling has not been established, but a first approach is as follows. Using the conventional strain-hardening expression for the cyclic stress–strain curve

$$\Delta\sigma = \Delta\sigma_0(\Delta\epsilon_p)^n \tag{9}$$

the assumption of an expression similar to the Griffith equation would result in

$$\Delta\sigma\sqrt{l_f} = \Delta\sigma_0(\Delta\epsilon_p)^n\sqrt{l_f} = B \tag{10}$$

In order to allow for some difference between the fracture law in the elastic range and that in the plastic range, we will assume that the relation in the plastic range is $(\Delta\sigma)^q\sqrt{l_f} = \text{const}$ where q is a constant yet to be determined. Thus, eq (10) becomes

$$(\Delta\sigma)^q\sqrt{l_f} = (\Delta\sigma_0)^q(\Delta\epsilon_p)^{qn}\sqrt{l_f} = B \tag{11}$$

Thus, substituting for l_f from eq (11) into eq (7), neglecting l_0, and applying eq (4), yield

$$\frac{2}{2-s}\,[B(\Delta\sigma_0)^{-q}(\Delta\epsilon_p)^{-qn}]^{2-s} = 2.5\ C(\Delta\epsilon_p)^s N_f^{2/3} \tag{12}$$

Combining terms involving $\Delta\epsilon_p$, we arrive at

$$\Delta\epsilon_p N_f^w = \left[\frac{2}{2-s}\,\frac{B^{2-s}(\Delta\sigma_0)^{-q(2-s)}}{2.5\ C}\right]^{\frac{1}{s+qn(2-s)}} = \text{const} \tag{13}$$

where

$$w = \frac{2}{3[s + qn(2 - s)]}, \quad s < 2$$

and where

- s = power-law exponent for crack-growth law; 1 if crack-growth rate is proportional to $\Delta\epsilon_p$ or $\sqrt{l}$
- n = strain-hardening exponent of cyclic stress–strain curve; between approximately 0.1 and 0.3
- q = modification factor for plastic fracture derived from Griffith equation for elastic fracture; 1 if same relation is followed plastically as elastically

A plot of w against nq for several values of s is shown in Fig. 41. It can be seen that, for $n = 0.2$ (an average value obtained from experimental data) and $q = 1$ (assuming an equation of the Griffith form to be valid), a value of $s \approx 1$ is required in order to make $w \approx 0.5$. It can also be seen that high values of s, for instance, above 1.5, would result in values of w well below the experimentally observed range, whereas values of $s \approx 1.0$ would produce very reasonable values. Thus, if this theory is correct, the implication is that, in the crack-growth-rate law [eq (5)], the crack-growth

rate is more nearly proportional to $\Delta\epsilon_p\sqrt{l}$ than it is to $(\Delta\epsilon_p)^2 l$.

It has already been observed that the case $s = 2$ cannot be treated in the manner just described, because of the logarithmic relation that develops during the integration of eq (6). The procedure can, however, be readily carried out, and computations show that the value of w is very close to $^1/_3$ for all values of nq, as would be implied by Fig. 41 for values of s that approach 2.0.

The preceding analysis introduces an interesting question regarding the crack-growth exponent. If the analysis is valid, it would appear that a value of s in the vicinity of 1.0 would best explain the relation between plastic strain and cyclic life. Experimental determinations would seem to point, however, to values of $s = 2$ as the more reasonable assumption, as noted, for example, in Fig. 38(b) where the logarithm of crack depth is plotted against percent life to obtain very nearly linear relations. The implication, then, is that the integration should involve a term log l, as would be obtained if s were equal to 2. The question revolves, however, about the meaning of the parameter, plastic strain range, when the crack is growing deep enough to be measurable. In our tests, we measure the diametral strain and maintain it constant even after the crack starts; in the last stages of the test, we maintain axial displacement constant. Thus, there is really no uniform plastic strain across the section when the crack is of appreciable measurable depth. If we consider only the limited region of l, for instance, less than 0.01, we have to question whether linearity in this range on a logarithmic scale [in Fig. 38(b)] has any real significance, and whether equally good linearity would not be obtained on other scales associated with other values of s. Thus, we conclude that the indirect method of determining s for this geometry by examining the exponent w might have some merit over the method of direct measurement. Since there are so many unanswered questions regarding the validity of all available analyses of the problem, it must be concluded that considerably more research is needed to clarify them.

An alternate approach that leads to acceptable values of the exponent in the power-law relation is to separate the exponents of ϵ_p and l in eq (5). For example, we could assume that

$$\frac{dl}{dN} = C(\Delta\epsilon_p)^t l^{s/2} \qquad (14)$$

and proceed in the same manner as before to integrate this differential equation. The final result, analogous to eq (13) is

$$\Delta\epsilon_p N_f^w = \text{const}$$

where

$$w = \frac{2}{3[t + qn(2 - s)]}$$

On this basis, there are a large number of admissible combinations of s and t that produce values of w in the desired range of 2/3. Specifically, for example, the simplest combination is for $s = 2$, $t = 1$. For these values, a logarithmic integration is required, resulting in the relation

$$\ln \frac{l_f}{l_0} = 2.5\, C\Delta\epsilon_p N_f^{2/3} \qquad (15)$$

The introduction of a fracture relation for σ_f analogus to eq (10) destroys the exact linearity of the logarithmic plot of $\Delta\epsilon_p$ against N_f, but the curvature involved is relatively small. In fact, the simplest procedure for interpreting eq (15) is to recognize that, for this combination of values of s and t, the curve of crack growth against number of cycles increases very rapidly in the region of failure. Thus, rather than introducing a failure criterion based on stress or $\Delta\epsilon_p$, we can say that failure will occur at the same value of l_f for all values of $\Delta\epsilon_p$; because of the steep slope of the $l - N$ curve, large differences between the true and assumed values of l_f will have a small effect on N_f. With l_f and l_0 having fixed values for a given material for all values of $\Delta\epsilon_p$, eq (15) states essentially that $\Delta\epsilon_p N_f^{2/3} = \text{const}$.

The purpose of the foregoing derivations is, of course, not to offer an accurate derivation of the power-law relation, but rather to indicate some of the component considerations that must be taken into account in such a derivation if it is based on the process of crack growth. The most important factor is the establishment of an accurate crack-growth law (preferably on a physical basis, but here arbitrarily hypothesized for simplicity); accounting for the nucleation period (i. e., not simply neglecting N_0, but somehow accounting for it); and finally establishing some basis for fracture (i.e., a criterion for choosing l_f). As long as all of these steps involve power-law relations, the final equation is in the form of a power-law relation between $\Delta\epsilon_p$ and N_f. By introducing eq (9), a corresponding power-law relation develops between stress range and cyclic life. Thus, the model hypothesized in Fig. 17, relating both elastic and plastic components to cyclic life becomes validated on the basis of these power-law relations.

Cumulative Fatigue Damage

The tests described so far relate to the behavior of material in which the independent variable, strain range, is maintained constant throughout the life of the specimen. When considering the behavior of actual structures, we must take into account operation under a spectrum of loading. This is normally referred to as cumulative fatigue. The classical linear damage rule first proposed by Palmgren[21], and later again by Langer[22] and by Miner[23], is now well known. It assumes that at any stage of the loading history of the material, the percentage of life used up is proportional to the cycle ratio at that loading condition. Thus, if a stress range or strain range is applied for n_1 cycles at a condition where

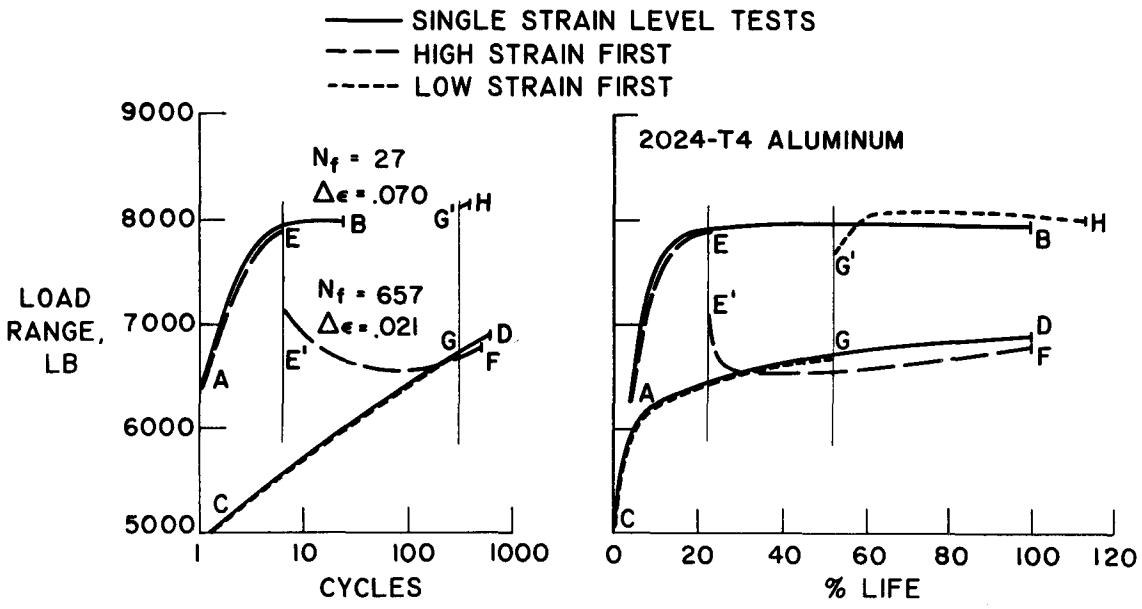

(a) Load range as function of number of cycles applied.

(b) Load range as function of percent of life.

Fig. 42—Cyclic strain hardening under two-level fatigue tests

failure would occur if N_1 cycles are applied, the percentage of life used up is n_1/N_1. That this is just an approximation and may often result in erroneous predictions of fatigue life is well known. Perhaps it would be appropriate to outline some of the factors that govern material behavior under cumulative fatigue loading and see wherein this rule tends to fall down, and to determine the requirements of a rule that would be more accurate.

Cyclic Hardening and Softening

Let us consider first the behavior of a material under cumulative fatigue loading as manifested by observation of its cyclic hardening and softening characteristics. Figure 42 shows some results obtained with 2024-T4 aluminum under an interrupted loading spectrum. The curve *AB* represents the load range plotted against cycles for a test in which the strain range is maintained constant at 0.070 and for which the life is 27 cycles. The curve *CD* represents a corresponding behavior when the strain range is maintained at 0.021 and the life is 657 cycles. Now if the test is conducted so that the strain range of 0.070 is applied for only 25 percent of the expected life for this strain level, it will be noted that, during this period, the variation of load range follows the curve *AE*. If at this time the strain range is changed to 0.021 and this latter strain range is maintained until failure occurs, the resulting load range curve is *E'F*. When examined in the type of plot shown in Fig. 42(a), the curve *E'F* appears somewhat complicated because, during the latter 75 percent of the test when the strain range is 0.021, the material first softens and then hardens. When viewed on the type of plot such as Fig. 42(b), however, this behavior becomes more understandable. Here, the horizontal scale is taken to be *percent* of life rather than cyclic life, otherwise the curves in both plots represent the same phenomena. It is seen that, initially the hardening from *A* to *E* follows the basic curve *AB*, as would be expected. When the strain range changes to 0.021, the stress range tends to fall within a relatively few cycles to the curve *CD* that corresponds to the same percentage of life that was already used up on curve *AB*. Thus, the curve *E'F* falls rapidly at first to curve *CD*, but since at 25 percent of the expected life the curve *CD* indicates the material is still undergoing considerable hardening, the curve *E'F* proceeds in a manner to indicate further hardening.

A similar result is obtained if one starts first with the low strain range and then continues the test at the higher strain level. To keep the curves separated we have chosen to illustrate the case in which half of the life is used up at the lower strain level, followed by straining at the higher level. The first portion of the test is represented by *CG*, which faithfully follows *CD;* the second follows the curve *G'H*. In Fig. 42(a), this segment is disconnected from the other curves and seems to bear little association to them. When plotted against *percent life* [Fig. 42(b)], however, the significance of *G'H* is made clear. It rises rapidly to the vicinity of curve *AB*, and follows it closely thereafter, indicating the validity of a linear cumulative life rule when considering the degree of hardening achieved at any point in the history of loading.

More extensive tests are shown in Fig. 43 for the same material. In Fig. 43(a), the results are shown for a change of strain level at approximately 25 percent of life for both a high- and a low-strain-level test. In Fig. 43(b), the change is made at approximately 50 percent of life and in Fig. 43(c) two

changes are introduced—one at approximately 25 percent and the other at approximately 50 percent of life. It is seen that in all cases the tendency is almost identical. Very shortly after the strain range is changed, the curve tends to seek a stress level corresponding to the curve for the new strain range at the percentage of life used up, regardless of the strain level at which the life fraction was consumed. Thus, the material may require initial softening to approach the necessary curve followed by hardening as it rises along that curve, or it may require initial hardening followed by subsequent softening for the same reason. These results are remarkably interesting because they imply that, at any condition of consumed life based on the linear damage rule, the material seeks a specific stress level associated with the cyclic hardening or softening curve connected with its *current* strain value and *consumed* life fraction. It is interesting to observe from Figs. 42 and 43 that, at fracture, the summation of the ratios is quite close to unity, as indicated by the end points of the test curves regardless of the sequence of loading.

Figure 44 shows the results of tests of this kind for a different material—a titanium alloy—which is basically strain softening. Here again, the curves can be followed through for the various tests indicated. The basic behavior is quite similar to that of a strain-hardening material previously discussed, but it will be seen that, when the change is made in strain level, the new stress sought by the material does not quite reach the curve associated with the new strain level. For example, in Fig. 44(a), if the high strain is applied for the first 24 percent of life, the curve follows segment AE. Changing to the lower strain level produces a point E' considerably below the curve CD at the 25-percent-life level. Further cycling at the lower strain level produces the curve $E'F$, which never quite reaches the curve CD. This behavior is characteristic of all the tests shown in this curve and requires further investigation.

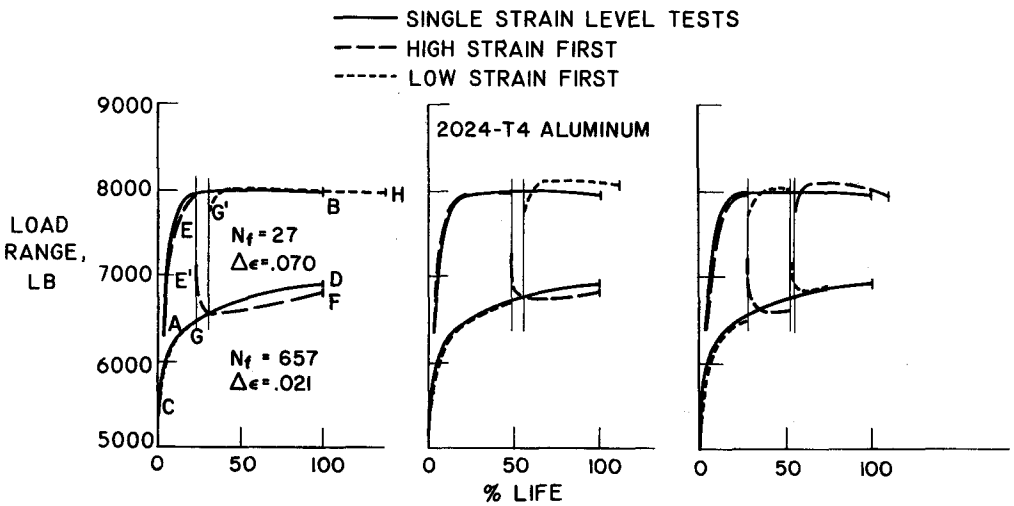

Fig. 43—Cyclic strain hardening under multilevel fatigue tests

(a) Single change of strain level at 25 percent of life.

(b) Single change of strain level at 50 percent of life.

(c) Strain levels changed at 25 and 50 percent of life.

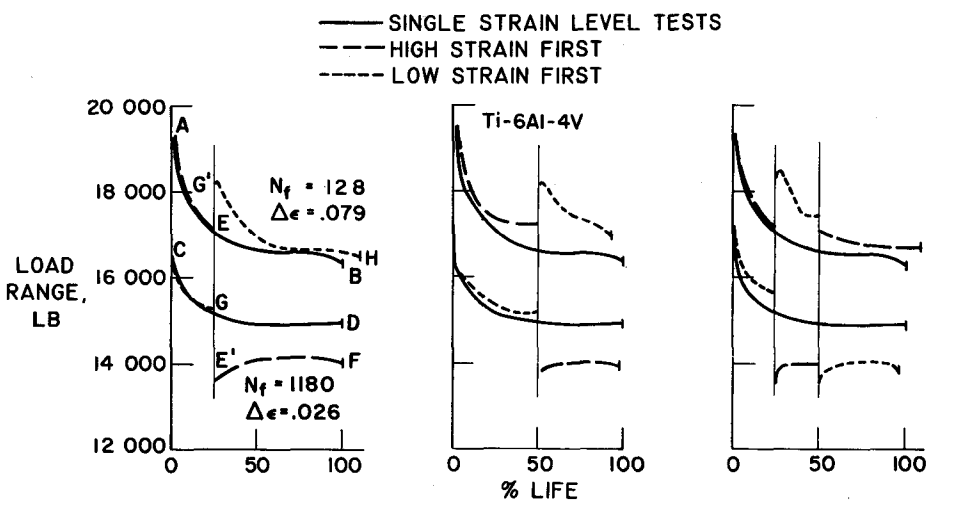

Fig. 44—Cyclic strain softening under multilevel fatigue tests

(a) Single change of strain level at 25 percent of life.

(b) Single change of strain level at 50 percent of life.

(c) Strain levels changed at 25 and 50 percent of life.

A summary of all of these tests on the basis of the linear damage rule is indicated in Fig. 45. Each set of horizontal lines represents one of the tests conducted. A step in the line indicates whether the high stress was applied first or last. Thus, for example, along the line for specimen L26, it is seen that the first 25 percent of life was at a higher strain level because this portion of the line is higher than the remaining portion. Fracture is indicated by the end point of each of these lines. It can be seen that, for all the tests summarized, the cycle ratio lies between approximately 0.8 and 1.3 and is very close to unity for most of the tests. Even the extremes are within the scatter band of expected behavior in this type of test.

These tests, therefore, would imply that the linear damage rule is quite accurate for these materials under the types of loading used. The significance of these observations in the light of what has already been said regarding the development and propagation of a crack is extremely interesting. In these tests, the main portion of the life was used up in developing a very small crack rather than in propagating the crack. It would appear, therefore, that as long as the major portion of the life is devoted to crack development, the linear damage rule might be applicable. It may be noted that this feature of assuming the validity of a linear damage rule within the crack initiation stage is inherent in the method developed by Grover[24] for the analysis of cumulative fatigue damage.

Aspects Relating to Crack Propagation

In the fatigue behavior of axially cycled small specimens, the propagation of a crack of engineering significance (i.e., longer than 0.003 in.) does not constitute a major portion of the life. In other cases, however, crack propagation might be much more significant. Let us consider, therefore, what the crack-growth curves should look like if they are to comply with the concept of the linear damage rule. Figure 46 shows the idealized crack-growth behavior if the crack length is regarded as the only

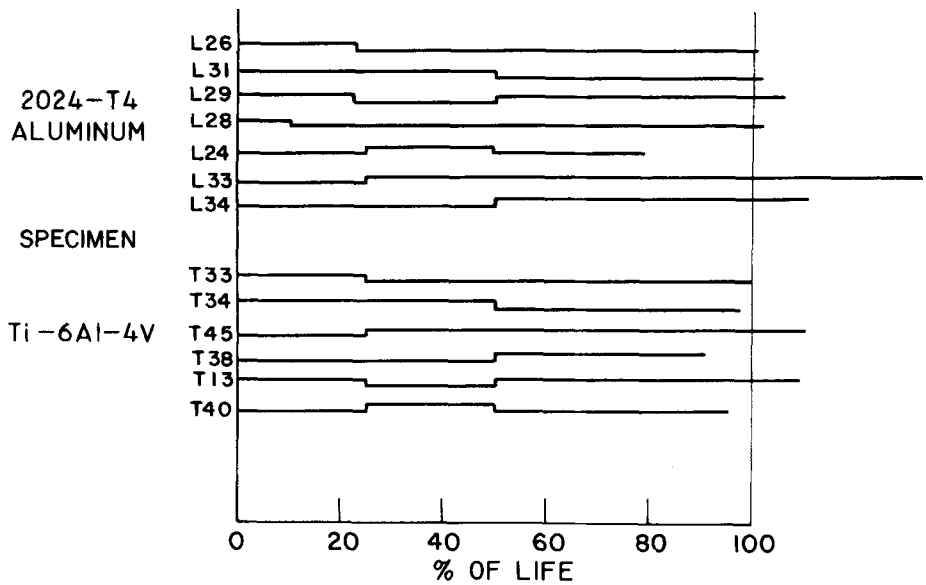

Fig. 45—Cumulative fatigue damage obtained by strain cycling of smooth specimens

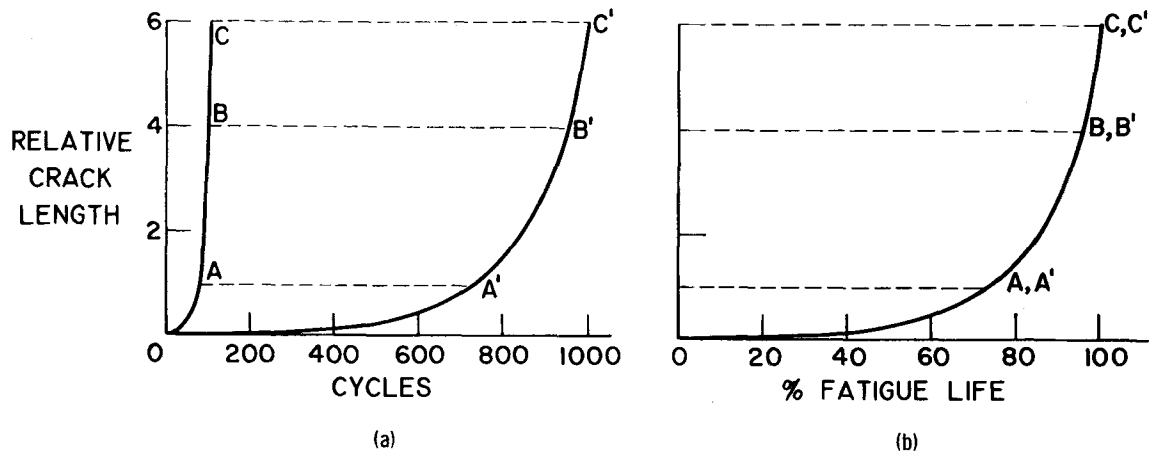

Fig. 46—Idealized crack-growth behavior satisfying linear damage rule

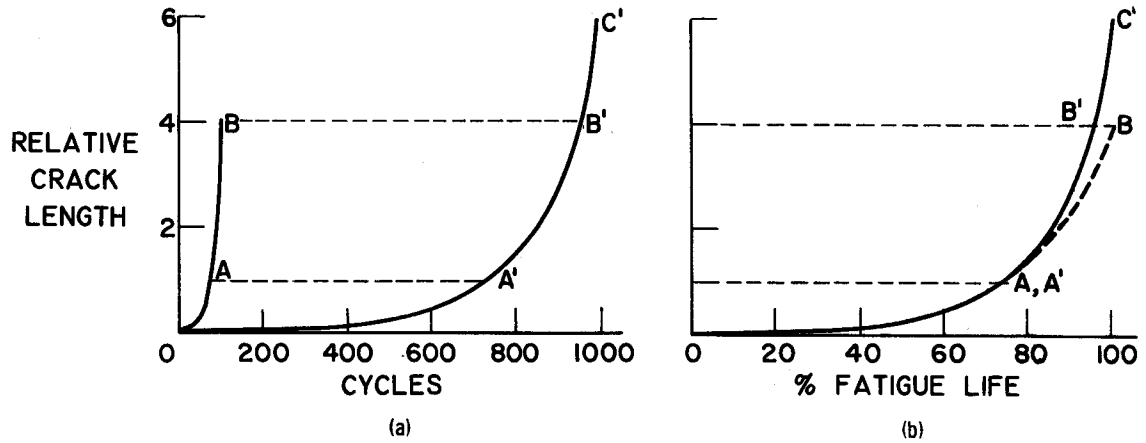

Fig. 47—Idealized crack-growth behavior showing need for deviation from linear damage rule

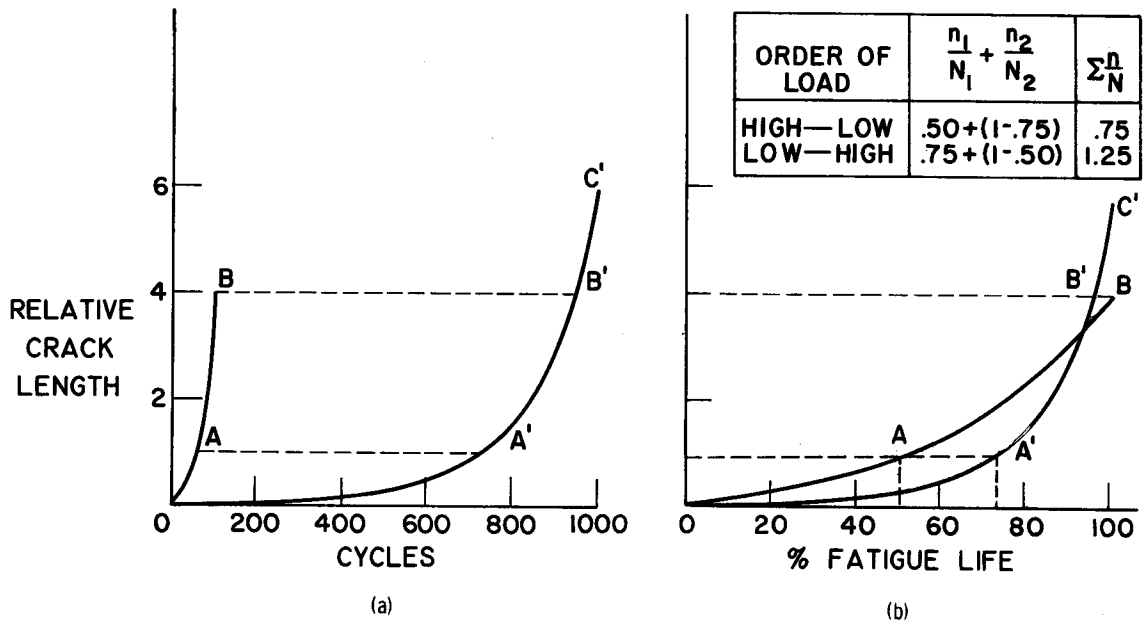

Fig. 48—Idealized crack-growth behavior complying with experimental trends

measure of material damage during cumulative fatigue tests. On the left of the figure is shown the idealized crack growth for two conditions of test, assuming lives of 100 and 1000 cycles. Curves $OABC$ and $OA'B'C'$ are the idealized curves for crack growth when the horizontal scale is plotted in actual cycles. If the curves are plotted on the basis of percent of life, as on the right of the figure, the assumption of a linear damage rule, together with the assumption that crack length is the only measure of fatigue damage, implies that both curves become coincident. Thus, point A will be at 75 percent of the hundred-cycle-life curve, $OABC$, while point A' will be at the 75 percent point of the thousand-cycle curve $OA'B'C'$. Similarly points B and B' must coincide, and C and C' must coincide. Since the crack-growth curves are of such a nature that they coincide when plotted on the basis of percent of life, then it does not matter whether one follows along the line OA and then moves to A' at a constant crack length, continuing the test from A' to C', or whether one follows from OA to AC along the same curve. Each piece of curve traversed between any two of the letters indicated represents the same fraction of life consumed.

It can be seen, however, that this idealization of the crack-propagation behavior is not possible. At least one reason is indicated in Fig. 47. The permissible crack length in a specimen before fracture occurs depends at least to a limited extent on the stress or strain that is being applied. Obviously, for a low stress range or strain range, a greater crack length will be permitted before fracture occurs. Thus, as seen in Fig. 47, the specimen with the 100-cycle life, implying a high strain range,

will fail at, for instance, a relative crack length of 4 at point B, while the high life specimen, implying a low applied strain range, will fail at a larger crack length of 6 at C'. When plotted on the basis of percent life to fracture, it becomes impossible for the two curves to coincide at all crack length levels because there is a region of crack length that corresponds to one of the curves that does not even exist in the other curve. At best, therefore, the kind of result that can be obtained is shown in Fig. 47(b). It is possible that a small region of the curve—perhaps from O to A,A'—can correspond to both the curves OA and OA' of the cyclic-life portion of Fig. 47; beyond this point, however, some deviation between the two curves must occur. Once the two curves are no longer coincident, the linear damage rule cannot apply because, at a given crack length, different percentages of life are used up depending on the strain level at which the crack was generated.

In reality, the problem is much more complicated than indicated in Fig. 47. The main problem is that crack length cannot be regarded as the sole measure of cumulative fatigue damage. Among other important factors are residual stress (especially in the vicinity of a propagating crack); metallurgical changes, particularly structural stability; the number of cracks present and their state of coalescence, etc. But even if we still continue to analyze cumulative fatigue damage on the sole basis of crack length, the linear damage rule is invalidated by failure of the crack-propagating curves to coincide, as shown in Fig. 48, when plotted on a basis of percent life. The basis for this lack of coincidence has already been indicated earlier when discussing the crack-growth curves for the polycarbonate resin in Fig. 38. It will be recalled that these curves were indeed plotted on the basis of percent of life and did not coincide. The curve for the low stress level indicates that the crack does not develop until much later in life, on a percentage basis. Once developed, the crack grows more rapidly when the plot is made on the basis of percent of life. This fact is illustrated in Fig. 48(b). The curves OAB and $OA'B'C'$ are realistic representations of crack-growth behavior for two strain levels. The crack-growth curve OAB for the high strain is steeper at the lower percentages of life, but terminates at a lower fracture-crack length. The low strain curve is flatter in the early percentages of life but becomes very steep in the terminal stages.

The significance of such behavior when viewed in the light of the linear damage rule can now be analyzed. Suppose, for example, the high stress is applied first along OA for 50 percent of the life. At this point, a change is made to the low strain range. If crack length is used as the only criterion of fatigue damage, assuming that a crack of a given length corresponds to a given amount of damage regardless of what strain level was used to induce the crack, then changing to the lower strain level implies a move to point A' and completion of the test to failure along line $A'B'C'$. At A', however, 75 percent of life has already been used up; therefore, the line $A'B'C'$ constitutes only 25 percent of life. The total life fraction used is thus 0.5 plus 0.25 as indicated in the table in Fig. 48(b), resulting in a cycle ratio of 0.75.

Reversing the procedure and applying the low strain range first to point A' produces a life fraction of 0.75. Changing to the high strain range implies a move back to point A, leaving 50 percent of life. Thus, a cumulative life fraction of 1.25 may be obtained as again indicated in the table. We see, therefore, that the order of application of the strains may seriously affect the summation of the cycle ratios. Applying the high strain range first followed by the low strain range produces a cycle ratio less than unity; applying the low strain range first followed by the high strain range produces a cycle ratio greater than unity.

Experience has verified this conclusion. Many tests have been conducted in which step functions in stress or strain have been applied. Two-step tests have been the most common. These tests, in general, have verified the conclusion that the order of application is important, and that when a low strain range is applied first less damage is incurred than when the high strain range is first applied. We have conducted many such tests in our own laboratory and this subject has been touched upon in some of our earlier publications.[25, 26]

An important deviation from this conclusion has, however, been observed in the testing of notched specimens. It has, in fact, been found that applying the high stress range first to such a specimen results in a higher cycle-ratio summation than applying the low stress range first. There are several reasons for this observation. Perhaps the most important is the fact that, when a notch or a crack is present, important residual stresses are retained when the cyclic load range is reduced from an initial high value to a low value. For example, for cyclic tests run from zero to tension only, when applying the high stress range first, a residual compressive stress is produced at the crack tip on unloading. A considerable number of cycles at a lower stress or strain range would then be required to overcome the residual stress field produced by the prior history. This behavior has been studied by Weibull[27] and others, and the delay time in continued cracking has been substantial when the high stress is first applied. This observation makes it clear why crack length itself cannot be considered as the only criterion for the existence of damage. At least the question of residual-stress field at the crack tip must be included.

There is, in addition, another reason for the ordering effect of load application observed in notched specimens. This reason will be illustrated with the use of Fig. 49. It will also be shown that, in two-level cumulative damage tests, one may reach a different conclusion as to the relative damage

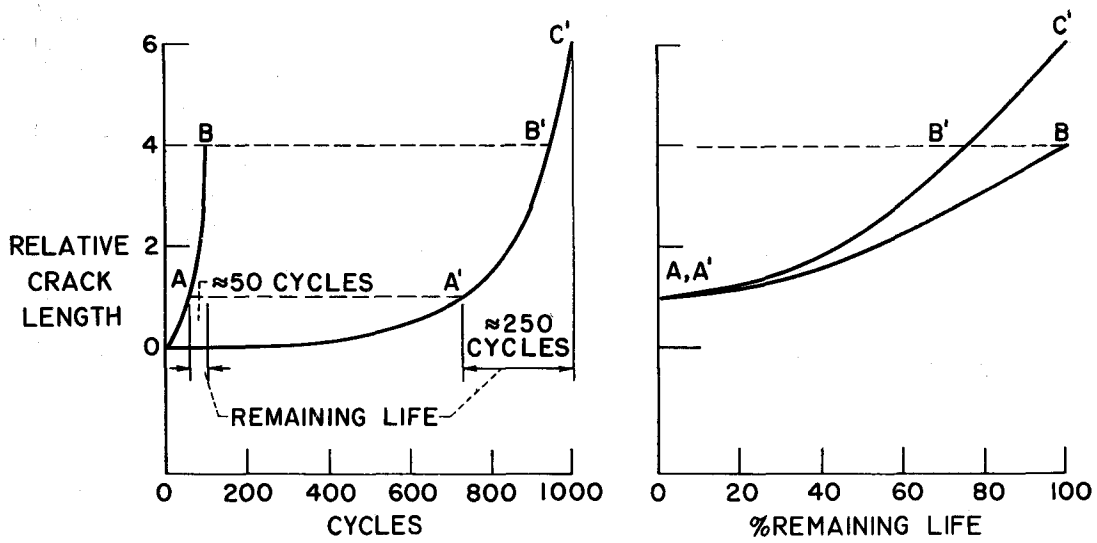

(a) Relative crack length as function of number of cycles applied.

(b) Relative crack length as function of percent remaining life.

Fig. 49—Idealized crack-growth behavior for precracked specimen

done by applying the high or low stress first, depending on whether a notched or unnotched specimen is being considered. This difference in behavior becomes obvious after a comparison is made of Figs. 48(b) and 49(b).

Consider, for example, the crack-growth behavior of a specimen with an initial crack length of one unit. This crack may have been generated by machining or by prior load cycling. Figure 49(a) shows how this unit crack length could be produced in an initially unnotched specimen under two arbitrary conditions of strain cycling. These growth curves are the same as those shown in Fig. 48(a) for the crack growth of unnotched specimens. Let us assume that the remaining lives of these two specimens with the unit length crack are 50 and 250 cycles, respectively. These may now be regarded as notched specimens having known fatigue lives (when cycled at the same strain used to produce the notch) of 50 and 250 cycles. What is important to this discussion of cumulative damage is the remaining crack-growth behavior of these specimens represented as a function of percent of life to failure, or percent of life remaining after the crack has been generated. This behavior is shown in Fig. 49(b). The crack-growth curves are shown as AB and $A'B'C'$, in which AB now lies entirely below $A'B'C'$. If an analysis were made of the effect of order of application of strain in a manner analogous to that discussed in connection with Fig. 48, it would be seen that the summation of the cycle ratios would be greater than unity if the *high* strain were applied first in notched specimens. This result is not related to any aspect of residual stress but is simply the consequence of the crack-growth behavior of a notched specimen (i.e., using the *remaining life* after the crack has reached an appreciable size in an initially unnotched specimen

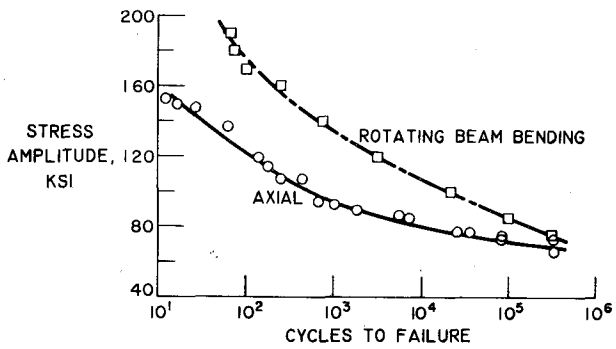

Fig. 50—Fatigue data under axial loading and in rotating bending for 4130 steel

as the basis for calculating cycle ratios). Obviously this effect may also be due to residual stresses and metallurgical effects, but it is of interest in understanding apparent inconsistencies in observations regarding the effect of order in the application of stresses or strains.

The subject of cumulative damage is covered by a vast literature. Further information on this subject may be found in Refs. 21 to 36.

Applications Involving Strain-cycling Data

Relation Between Axial and Bending Fatigue

The significance of the studies of materials in strain cycling will now be illustrated by a very simple application that can also be extended to more complicated problems. In this application, we have concerned ourselves with the relation between the axial-fatigue behavior of materials and their bending-fatigue behavior.

It is well known that metals have longer lives

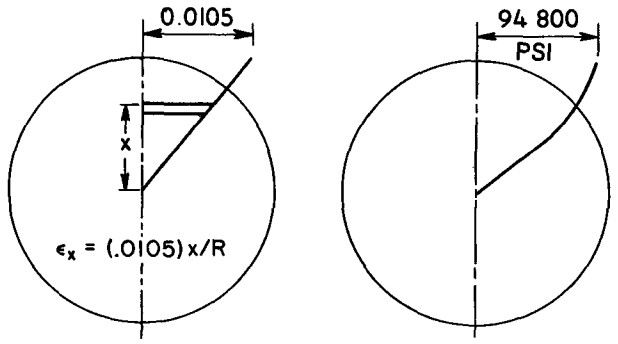

(a) Strain distribution for life of 1000 cycles.

(b) Stress distribution from (a) and cyclic stress-strain curve.

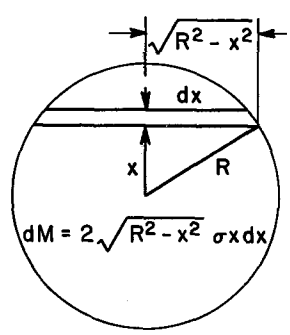

(c) Contribution of strip to bending moment.

Fig. 51—Determination of bending moment supported by circular section for selected value of surface strain

$$M = 2\int_0^R dM = 4\int_0^R \sqrt{R^2 - x^2}\,\sigma x\,dx =$$

113,000 in.-lb

when tested in bending fatigue for the same *nominal* stress level than they have in axial fatigue. This fact is illustrated in Fig. 50. Here the fatigue lives of specimens of 4130 steel were obtained by two different methods. The lower curve is the saturation stress range plotted against the cyclic life when the strain range is axially applied and, therefore, approximately uniform over the entire cross section. The upper curve refers to rotating-beam specimens. The stress plotted is the nominal value obtained from the elastic-bending-moment formula $S = Mc/I$. Obviously there is a considerable difference between these two curves.

A question arises as to the reason for this difference. One reason obviously is that the formula, which assumes elasticity, is not accurate, especially in the low-cyclic-life range where the strains are well into the plastic range. Thus, in this example we shall investigate whether the axial- and bending-fatigue results would be the same if the actual stress or strain in the rotating-beam specimen were known.

As shall be indicated later, the question of rotating-beam bending is much more complicated than appears upon first examination, and we shall therefore look first at a similar problem which is introductory to the study of rotating beams. Instead of considering a specimen which is flexed during rotation, let us consider first a round specimen subjected to simple reverse flexure. Imagine the specimen to be bent back and forth about a fixed axis. The basis for the analysis is indicated in Fig. 51. If we try to solve the problem by selecting a bending moment and determining the corresponding surface strain range, we encounter difficulties in solving the complicated nonlinear equation that results. To avoid these difficulties, we select instead the surface strain (which, in turn, establishes the life) and seek to determine the bending moment that will produce the selected surface strain. This can readily be done as illustrated in Fig. 51. For example, if we select a surface strain of 0.0105 and make the assumption, commonly made in bending analysis, that plane sections remain plane, the strain is known at every point in the specimen cross section. At any vertical distance x from the center of the specimen, the strain is $0.0105\ x/R$ as shown

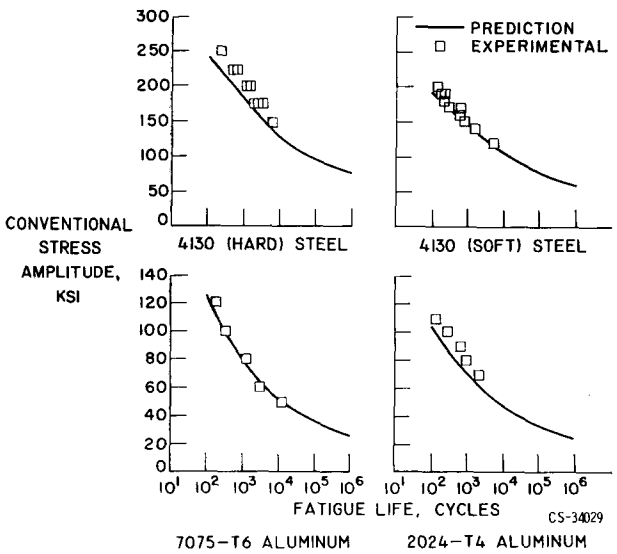

Fig. 52—Prediction of flexural fatigue from reversed axial strain-cycling behavior

in Fig. 51(a). Knowing the strain range at each location, and having available a cyclic stress–strain curve that relates the strain range to the stress range, we may then determine the stress range at each location in the cross section. This is illustrated in Fig. 51(b). For the materials selected, the surface stress is 94,800 psi and the stresses at all other distances from the axis toward the center are displayed by the curve shown. The contribution to the bending moment associated with each stress can be determined from the product of the area over which the stress acts and the distance from the bending axis. This is illustrated in Fig. 51(c). On carrying out the indicated integration, we conclude for the example shown that the bending moment is 113,000 in.-lb. Once the bending moment is known, we can then determine from the equation $S = Mc/I$ what the nominal bending stress would have been for this bending moment. In this way it is possible to make a plot of the applied nominal stress against predicted life and compare it with experimental data.

Results for several materials are shown in Fig. 52. The continuous lines refer to predictions deter-

mined by the described procedure, and the experimental data points are for tests conducted to determine the validity of the predictions. It can be seen that the agreement for the two steels and two aluminum alloys is quite good. In general, the predictions are somewhat conservative. The reason for this is that the predictions are based on axial-fatigue data in which the crack-growth stage is, as already discussed, a relatively small part of the total life. In the bending tests, the crack-growth stage is longer. Therefore, the assumption that failure occurs soon after the crack starts is somewhat conservative for the bending tests, and the predictions are also conservative. Another reason for the discrepancy, perhaps a minor factor, is the assumption that, throughout the life, each point is at the saturation stress level associated with its strain value. This is a reasonable assumption for the outermost fiber where the strain is a maximum (recalling that saturation is achieved early in the cyclic life when the entire section is subjected to the same stress and recognizing also that the life is to be governed by the strain at the outermost fiber). The assumption is not valid, however, at points of lesser distances from the neutral axis, which are subjected to lower strains, and for which a larger number of cycles are required to establish saturation stresses. Still another reason for the discrepancy is the unknown effect of strain gradient on life. In the axial strain-cycling tests, the strain is uniform over the entire section, whereas in the bending tests, only a very small region at the outermost radius is at the maximum strain, while the remainder of the section is at lower strain. Nevertheless, despite the many factors that could cause discrepancy, the agreement between predictions and experiment shown in Fig. 52 is seen to be very good.

We can now proceed to examine the more complicated case of rotating bending. Before doing so, let us recognize that the reason the case of flexural bending lends itself so easily to analysis is that, once the surface strain has been assumed, all stresses and strains in the cross section are immediately established, since they are all in phase, reaching a maximum amplitude at the same time. Figure 53 shows the complication that develops when considering rotating bending in contrast to flexural bending. Consider the two elements A and B shown in Fig. 53(b). If the cross section were simply being bent back and forth as in flexural bending, these two elements, being at the same distance from the bending axis, $\alpha - \alpha$ would have exactly the same stress. In rotating bending, however, the problem develops because of a phase relation, with the result that A and B are not at the same stress level, unless the entire cross section is elastic. If we were to analyze this problem in the same manner as we did for flexural bending, assuming a strain at the surface of ϵ_0, the stress at points A and B would be equal and would be obtained from a knowledge of the strain, as shown in Fig. 53(c). If the cross section were not rotating, A and B would always be at the same distance from the neutral axis, as shown in Fig. 53(b), and no question would arise regarding the value of stress in these elements. When we consider rotating bending, however, it is clear that points A and B will *ultimately* reach a strain level ϵ_m when they achieve the maximum distance from the strain axis, but that at the instant considered in the figure, point B has already passed its maximum strain, while point A is approaching its maximum. The stresses at each of these points must be determined from the hysteresis loop [Fig. 53(d)]. In this figure, the stress corresponding to the maximum strain ϵ_m to be reached by both these points is shown as σ_m, obtained from Fig. 53(c) for the maximum strain ϵ_m experienced by both points A and B. To obtain the current stresses, however, we must determine the stress when the strain is ϵ. Therefore, referring again to Fig. 53(d), we can move out a distance ϵ from the vertical axis locating the points identified as σ_A and σ_B. These are the stresses at the two elements A and B. Thus, even though A and B are at the same distance from the strain axis, their stresses are, in fact, quite different at the instant considered and, in obtaining the bending moment, allowance must be made for the actual stress present in each element.

Further reflection regarding this problem indicates that the best approach for analysis is that indicated in Fig. 54. The loading axis xx is the axis about which the bending moment is applied. If one considers the strains at the individual locations in the element, it can be seen that the cross section bends about a *different axis* $\alpha\alpha$, which makes an angle φ with the xx axis. By writing an expression for the bending moment contributed by all

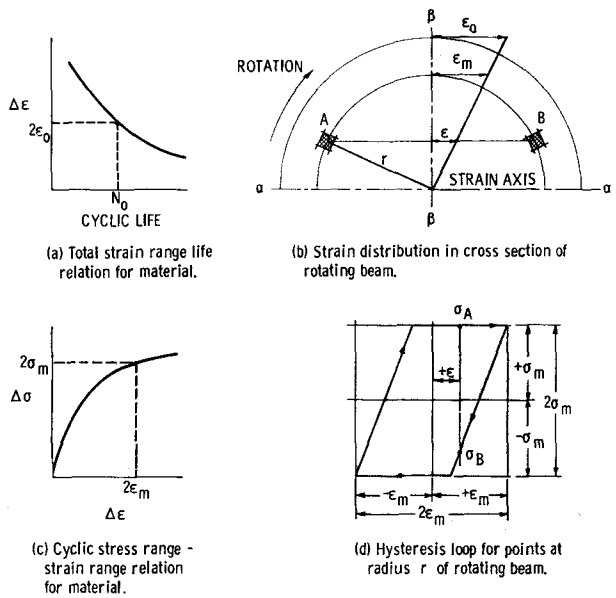

(a) Total strain range life relation for material.

(b) Strain distribution in cross section of rotating beam.

(c) Cyclic stress range - strain range relation for material.

(d) Hysteresis loop for points at radius r of rotating beam.

Fig. 53—Determination of stress distribution in a rotating beam from axial strain-cycling-fatigue data

$$M_{\alpha\alpha} = \Sigma\sigma \cdot \beta \cdot \Delta A = \Sigma\sigma \cdot r \cdot \sin\theta \cdot \Delta A$$
$$M_{\beta\beta} = \Sigma\sigma \cdot \alpha \cdot \Delta A = \Sigma\sigma \cdot r \cdot \cos\theta \cdot \Delta A$$
$$M_{yy} = \Sigma\sigma \cdot \chi \cdot \Delta A = \Sigma\sigma \cdot r \cdot \cos(\theta + \varphi) \cdot \Delta A$$
$$= \Sigma\sigma \cdot r \cdot \left[\cos\theta \cdot \cos\varphi - \sin\theta \cdot \sin\varphi\right] \cdot \Delta A$$
$$= \cos\varphi \cdot M_{\beta\beta} - \sin\varphi \cdot M_{\alpha\alpha}$$

BUT $M_{yy} \equiv 0$

$\therefore$ HYSTERESIS ANGLE $\varphi = \tan^{-1}\left(\frac{M_{\beta\beta}}{M_{\alpha\alpha}}\right)$

$$M_{xx} = \Sigma\sigma \cdot y \cdot \Delta A = \Sigma\sigma \cdot r \cdot \sin(\theta + \varphi) \cdot \Delta A$$
$$= \Sigma\sigma \cdot r \cdot \left[\sin\theta \cdot \cos\varphi + \cos\theta \cdot \sin\varphi\right] \cdot \Delta A$$
$$= \cos\varphi \cdot M_{\alpha\alpha} + \sin\varphi \cdot M_{\beta\beta}$$

NOMINAL $\sigma_{MAX} = M_{xx} \cdot \frac{R}{I} = \frac{4M_{xx}}{\pi R^3}$

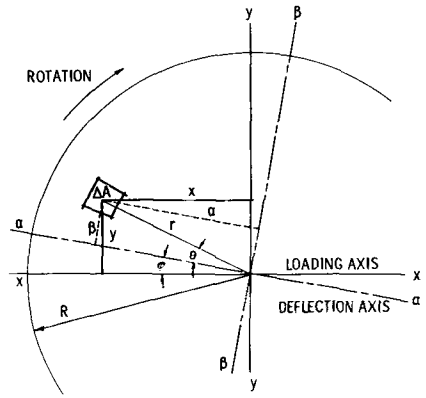

Fig. 54—Determination of bending moment and hysteresis angle in a rotating beam

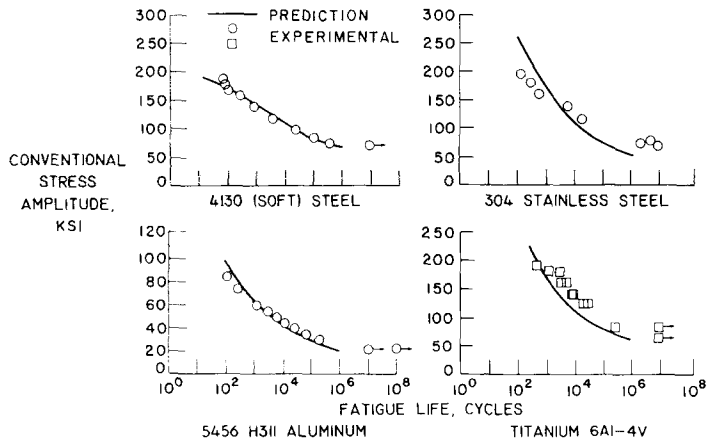

Fig. 55—Prediction of rotating-bending fatigue from reversed strain-cycling behavior

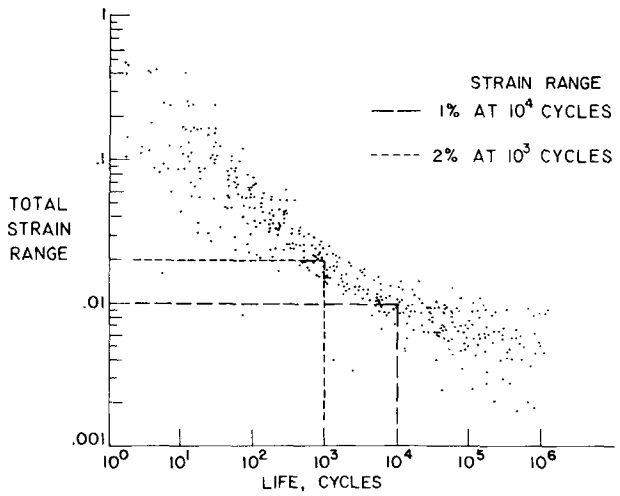

Fig. 56—Axial strain-cycling-fatigue behavior of 29 materials

the elements about an arbitrary axis relative to the displacement axis, and expressing the fact that the bending moment about the axis normal to the loading axis *xx* must be zero (since the applied bending moment has no component about this normal axis), we can determine the angle φ between the deflection axis and the loading axis, as shown in the figure. The computations are somewhat complex, and details will be provided in a forthcoming NASA publication. Once the angle between the two axes has been determined, the complete stress and strain distribution can be computed, from which the bending moment for an assumed value of maximum surface strain can be established. From the assumed value of surface strain, life can be determined from Fig. 53(a).

A comparison of the predicted results and experimental data is shown in Fig. 55. The curves are the predictions based on axial-fatigue data; the experimental data are indicated by the symbols. The comparison is quite good, certainly much better than the agreement shown in Fig. 50. Thus, it can be concluded that one of the main reasons why bending and axial fatigue do not agree is that we do not, in reality, know what the true strain is on the surface for a given applied bending moment in rotating bending. When the proper surface strain is determined by an analysis of the type indicated here, greatly improved results are obtained.

The problem discussed here is obviously an extremely elementary one, but the basic approach involving the use of the cyclic stress-strain curve can be extended to much more difficult and more general problems.

Rule of Thumb Relating Strain Range to Cyclic Life

In an earlier publication,[14] it was observed that, as a first approximation, most materials will survive approximately 10,000 cycles of application of a strain range of 1 percent. Morrow[37] has examined this rule of thumb in comparison with others and has concluded that an even better rule is one suggested by Peterson[38] that most materials can withstand 1000 cycles of a strain range of 2 percent prior

to failure. Because of the large amount of data recently developed in our laboratory relating life to strain range, it is appropriate to re-examine both these rules.

The results for the 29 materials previously used in our discussion are shown in Fig. 56. Here all the data are shown in a plot of strain range against life, regardless of the values of tensile strength and ductility of the individual materials. It is seen that in the low life range there is considerable spread in the points because of the large range in ductilities of the materials; in the very long life range, a spread again develops because of the large range in the strength levels of the materials tested. In the range between 1000 and 10,000 cycles, the spread narrows considerably, and each of the two rules cited above presents a reasonable approximation of actual material behavior. (The very discrepant data points in the low-cyclic-life range refer to the powder-metallurgy-produced beryllium, which probably did not reach its full potential in fatigue.) If a rigid choice had to be made between the merits of the two rules, it would probably be in favor of the 2 percent rule at 1000 cycles, but both rules are useful for establishing the approximate behavior in the range of life between 1000 and 10,000 cycles.

Fundamental Aspects of Fatigue

As has already been indicated, it is not the intention here to summarize the state of knowledge of the fatigue mechanism, since this subject is not only too broad, but also because many good summaries have recently appeared. However, some of the aspects of the subject that have been discussed from an engineering point of view also have some fundamental significance that bear summarization. In the following discussion we shall limit ourselves primarily to results that have already been mentioned in some other connection, introducing only a few additional features needed to round out the interpretation of these results.

Cyclic Strain Hardening and Softening

The first feature in the fatigue process that we have observed in our discussion is the change in stress range required to maintain a given cyclic strain range. The features of major significance associated with such cyclic hardening or softening are summarized in Table 3. First, we have noted, as in Fig. 8, that such changes in stress are manifestations of microstructural changes. Since these changes are an indication of the rather large possible changes in the yield point, it can be seen that the *initial* yield point is of relatively little significance in governing the fatigue behavior when large plastic strains are involved. The validity of this implication has been demonstrated by showing that the fatigue life in the low- and intermediate-cyclic-life range depends very little on the initial yield point. We have also indicated that saturation hardening or softening occurs relatively early in the life of a specimen, as illustrated in Figs. 15(c) and 16(c), as long as the strain range is maintained constant during the complete history of loading. When changes are introduced in the strain range during the course of the life of a specimen, these changes may be accompanied by large changes in hardening or softening; the material seeks a new stress level which would place it on the hardening or softening curve associated with the new strain level. The point on the curve it seeks depends roughly on the sum of the cycle ratios of the prior history. Thus, as indicated in item (4) of Table 3, we conclude that changes in stress are governed approximately by a linear life-fraction rule. Limited evidence of this behavior is shown in Figs. 42 to 44, but more data are needed for more general substantiations. Finally, we observe, as in item (5) of Table 3, that cyclic hardening and softening may appreciably alter the macroscopic *stress distribution* in an engineering structure, since the stress distribution depends on the cyclic stress-strain curve, which in turn is influenced by the hardening or softening. An example of this effect has been discussed in connection with the bending problem, where it has been indicated that computations using the cyclic stress–strain curves lead to improved determination of the actual surface stresses and strains, which make possible a more accurate determination of life.

TABLE 3—CYCLIC STRAIN HARDENING AND SOFTENING

(1) Manifests microstructural changes

(2) Tends to wipe out initial yield point

(3) Usually approaches saturation early in life

(4) Changes in strain level result in stresses governed approximately by cumulative linear life-fraction rule

(5) Influences macroscopic stress distribution (rotating and flexural bending)

Microstructural Events in Fatigue

The microstructural events associated with hardening and softening, and which lead to the eventual development of a crack that can then start propagating in subsequent cycling, are outlined in Table 4. As indicated in item (1), the most important factor to bear in mind in connection with fatigue is that, in crystalline materials, plastic deformation of any one crystal can for the most part take place only in a few, well-defined directions associated with the slip planes. While the

TABLE 4—MICROSTRUCTURAL EVENTS IN FATIGUE

(1) Slip on a few well-defined planes tends to produce internal discontinuities

(2) Substructure formation helps maintain continuity; it results, however, in more centers of disorder

(3) Slip may affect the nature of the microstructure, for example, break up dispersed particles (strain softening)

(4) Slip not completely reversible, results in internal and surface discontinuities

equations of compatibility (those equations that result from the assumption that the material remains continuous) stipulate a strain distribution in *all* directions, such strains may not be possible when the available directions of slip are limited. Thus, if the strain develops only as a result of slip on such a limited number of slip planes, there develops a tendency to create points of material discontinuity. Naturally, the more grains there are per unit area, each grain being differently oriented so that its slip planes are in different directions, the easier it becomes to satisfy the compatibility requirements without producing localized points of discontinuity. For this reason, as indicated in item (2) of Table 4, and demonstrated in Fig. 8, a *substructure* develops within the individual grains. That is, the grains subdivide into smaller regions, each having a slightly different orientation relative to the adjacent regions, so that its slip planes are in a different direction. Thus, there is established a greater ease of obtaining a required plastic-strain distribution. Such realignment of the subgrains is not, however, accomplished without paying a price. This price is in the form of greater disorder in the subgrain boundaries,[39] which eventually may serve as nuclei for fatigue cracking, but at least in the early stages must be regarded as beneficial.

While cyclic strain hardening can readily be interpreted according to accepted concepts involving the exhaustion of planes of easy slip, the pile-up of dislocations, or any other mechanism that requires more force to cause a given amount of slip after slip has already occurred previously, strain softening is somewhat harder to understand physically. Item (3) of Table 4 indicates one mechanism for strain softening that is applicable to dispersion-strengthened materials (materials that gain their strength as a result of a dispersion of very fine, hard particles, such as carbides in steel and oxides in aluminum). McEvily and Boettner[40] have found, for example, that in an aluminum alloy which gains its strength in this manner, cyclic straining caused the hard, brittle particles to be broken up whenever slip occurred along a plane intersecting them. Eventually, the particles become so small that they become unstable in their matrix. When the particles become small enough, the ratio of their surface to volume becomes very high, and they become unable to resist dissolution into the surrounding matrix. As the particles dissolve, the region becomes soft because of the removal of the hardening agents, thus explaining a mechanism of cyclic strain softening. Other explanations are, of course, required for other systems. The distribution of dislocations associated with strain hardening in static loading may, for example, be unstable when the material is subsequently subjected to cyclic plastic strain. A new dislocation structure and distribution may thus develop that more readily lends itself to slip, producing strain softening. Softening may also be a manifistation of the relief of residual stresses.

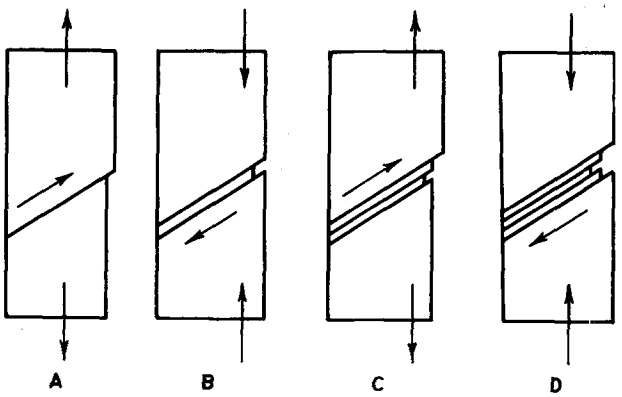

Fig. 57—Schematic view of crack nucleation. (Wood, 1958)

The final item, item (4) of Table 4, refers to a mechanism whereby a crack is eventually developed as a result of cyclic reversal of strain; it has been proposed by Wood,[41] among others, and is illustrated in Fig. 57. The concept is associated with the (at least partial) irreversibility of slip of any one slip plane. In Fig. 57(a), slip takes place along one slip plane when the load is tensile as shown. Reversing the load does not reverse the slip on the identical plane; at least a part of the reversed slip takes place on an adjacent parallel plane, producing a small notch at the surface (or in the interior at a grain boundary in some cases), as shown in Fig. 57(b). Further cycling enlarges the discontinuity, as shown in Figs. 57(c) and (d), eventually developing a crack of macroscopic proportions that responds to engineering formulas for strain concentration in the vicinity of a notch, thus further aggravating strain localization. A notch such as that shown in Fig. 57(d) has been called an intrusion, because of the absence of material; when the slip is of such nature as to form an excess of material jutting out from the surface, it is called an extrusion. Examples of such extrusions have been illustrated in Fig. 13.

Development of Microcracks

Further aspects of the development of microcracks are outlined in Table 5. As noted in item (1), such microcracks may develop at regions of strain concentration associated with intrusions and extrusions already discussed, but they may also

Fig. 58—Crack propagation along slip lines in aluminum (Schive, 1964)

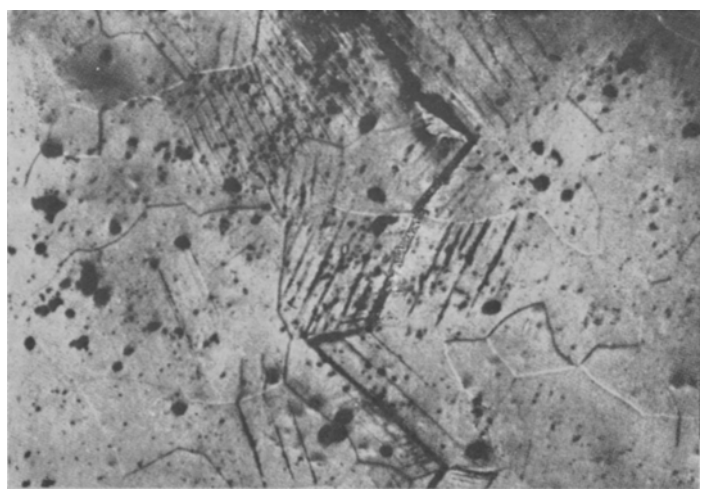

TABLE 5—DEVELOPMENT OF MICROCRACKS

(1) Influenced by initial surface topography, intrusions, extrusions, inclusions, flaws, grain boundaries, subgrain boundaries, twin boundaries, etc.

(2) Initial direction parallel to slip planes; stage I

(3) Slow growth; limited within individual grains; may stop at grain boundary or other impediment (nonpropagating crack)

(4) Main fraction of life used up in this stage, except at extremely high strain and low life

(5) Materials of high strain capacity (high ductility for plastic strain, high tensile strength for elastic strain) resist early development of microcracks

(6) Tends to follow cumulative linear life-fraction rule

develop at other regions of discontinuity such as surface irregularities, inclusions or other internal flaws, at grain boundaries, subgrain boundaries, twin boundaries or wherever a discontinuity of slip or slip direction occurs. As already indicated in Fig. 57, the initial direction of the crack is likely to be parallel to a slip plane, which is further illustrated in Fig. 58, taken from a recent report of Schijve.[42] The slip planes are delineated by the fine lines, and the crack by the coarse line. Note that, in any one grain, the crack is parallel to the slip plane and that, as the crack moves to an adjacent grain, it changes its direction so as to be parallel to the slip planes of the new grain. (Such parallelness is typical, however, only for the earliest stages of cracking. Cracking in the later stages is transcrystalline, with relatively little regard for the direction of the slip planes.) The early stages of cracking, wherein the crack is confined largely to an individual grain, or to a few adjacent grains, has been classified as stage I by Forsyth and by others. As indicated in item (3) of Table 5, the growth of such a single-grain-confined crack is quite slow. When it reaches a grain boundary it may, in fact, be stopped if the orientation of the slip planes of the adjacent grain is such as to fail favoring propagation. Many examples have been cited in the literature of so-called nonpropagating cracks, at least some of which may be explained on the basis of the favorable orientation of adjacent grains so as to prevent crack extension once the grain boundary or other impediment is reached.

Item (4) of Table 5 refers to the conclusion drawn from Fig. 39 that the major portion of the life is used up in initiating the crack. Because this conclusion may appear to be in contradiction to many current concepts that fatigue is predominantly the process of propagating a crack, it is important to clarify the significance of this item in order to avoid undue dispute in cases where no real conflict exists. First, we must recognize that the conclusion relates to cyclic lives greater than about 500 cycles. In the very low life range, Fig. 39 shows that crack propagation consumes, in any case, the major part of the life. At a life of 100 cycles, for example, only about 40 percent of the life is required to initiate the crack under consideration, and about 60 percent is required to propagate it to final fracture. Secondly, we must recognize that we are dealing with originally smooth specimens, wherein initially there are no gross strain-concentrating conditions. If a sharp discontinuity is initially present, the crack may develop and start to grow much earlier in the life. That this is the case has been illustrated in Fig. 14, where the specimen initially contains a very sharp notch, and it can be seen that a crack of about 0.0025 in. is detected within about 1 percent of the life almost over the entire life range for the specimen. Furthermore, we must recognize that we are concerned with small specimens of $^1/_4$-in. diam circular cross section, avoiding stress-corrosion conditions or other hostile environments that might be typical of service applications. Finally, and perhaps of the greatest importance, we must recognize that when we talk about a crack we mean one at least equal in size to the natural imperfections present on the surface of engineering materials. Any smaller cracks will have an insignificant effect compared with the imperfections already present. Undoubtedly, "cracks" developed by fatigue can be detected in highly polished laboratory samples earlier than shown in Fig. 39 if use is made of the very high magnifications associated with electron microscopy or of a high-power optical microscope together with "taper sectioning". Many investigators have observed "cracks" by such techniques very early in the life of a specimen, and their observations are not in dispute. It must be recalled, however, that the uses to which the curve of Fig. 39 was applied were associated with engineering problems rather than with their interpretation from the standpoint of physics. When considering notch sensitivity, which was the first application involved, it would seem reasonable that we would want to consider cases only when the crack is large enough to affect this sensitivity in an engineering sense, as already discussed. In the second application, that of considering the crack-growth law, we were concerned with writing an equation for crack growth during its "measurable" stage—whether by "striations," "ripples" or otherwise. We needed some boundary conditions for integrating the equations, and wanted to ensure that the corresponding values of l_0 and N_0 were within the range of validity of the observed crack-growth law; thus, we chose a value of l_0 that was within the "striation" stage which we were trying to analyze. Questions arising out of item (4) of Table 5 should therefore be answered only in relation to the purpose intended to be resolved, rather than to the academic question of the definition of a fatigue crack.

Item (5) of Table 5 gets at the heart of the relations sought for predicting both the elastic and plastic lines of Fig. 17 in terms of the ductility and tensile strength. By showing that these two properties are predominantly effective in governing the cyclic lives of small smooth specimens, we may conclude that the important factors governing the initiation of a crack and its very early stages of propa-

gation are the manifestations of the capacity of a material to deform. Thus, high ductility, which means high capacity for *plastic* deformation, and high tensile strength, which is a manifestation of the capacity for *elastic* deformation, are important characteristics that influence the ability of the material to resist crack initiation and early stages of crack propagation.

Item (6) of Table 5 refers to the results of Fig. 45 where, on a limited scale at least, it is seen that a cumulative linear life-fraction rule is valid when the major portion of the life is involved in initiating the crack. The complexities associated with the crack itself, high localization of strain, residual stresses, etc., destroy the validity of the linear damage rule, but up to the point where the crack is of sufficient size to introduce such complications, it would appear that such a linear damage rule may be applicable. Of course, more data than those shown in Fig. 45 are required for conclusiveness, and, of course, we implicitly assume that the material remains metallurgically stable, and that rate effects (e.g., creep) are absent.

Stage II Cracking

Table 6 summarizes some important aspects of crack growth once it has reached an appreciable length, and when the failure-propagation mode is one whereby progressive opening of the crack occurs normal to the direction of loading. This period has been called "Stage II cracking" by Forsyth.[43] As indicated by item (1), the crack now moves easily across grain boundaries and assumes the characteristic transcrystalline nature typical of fatigue failures. The factors that govern the extent of crack growth per cycle, and why in fact it grows only a certain distance in one cycle, while extending farther in the next cycle even though the nominal loading has not changed, have not yet been completely resolved. One explanation that has been offered is based on the concept of blunting and resharpening of the crack,[44] as indicated in item (2) of Table 6. Presumably the crack grows during the tensile portion of the cycle until the radius at the root of the crack increases (blunts) enough to relieve the stress concentration sufficiently so that no further crack growth is needed, at which time crack growth stops. The compressive portion of the cycle sharpens the crack, so that upon re-application of tension, further crack growth is needed to relieve the stress concentration again; however, this concept provides only a partial explanation. Of great interest would be an analysis involving the residual stresses because these stresses undoubtedly enter into the consideration of the amount of crack extension, but a proper analysis is as yet not available.

Item (3) of Table 6 relates to the characteristic of stage II cracking involving the merging of independently formed cracks. Except for cases involving very high cyclic lives, fatigue usually involves not one crack but many independently

TABLE 6—STAGE II CRACKING

(1) Crack penetrates grain boundaries; assumes characteristic transcrystalline nature
(2) Mechanism of crack growth may be related to blunting and sharpening of crack under tension and compression
(3) Independently formed cracks merge
(4) Power laws of crack length and of plastic strain describe crack growth
(5) Not governed by linear life-fraction rule.
(6) Residual stress induced by prior stress history is important

formed cracks that merge, and crack growth, in part, consists of the merging of such cracks rather than just the propagation of a single crack. Most analyses of crack growth do not, however, take such type of crack growth into consideration.

As indicated by item (4) of Table 6, the rate of crack-length growth during stage II cracking is governed by power laws of crack length and plastic strain. Thus, when the crack is small, the growth rate is also small; as the crack length increases, its growth rate also increases rapidly, so that in the latter part of the test the growth rate may become catastrophically high compared with the rate in the early part of the test. Here also, is a partial explanation of why notch sensitivity does not significantly affect the fatigue characteristics in tests of the type used to establish the life relations discussed in this report. The less notch sensitive the material, the deeper is the crack that can be withstood before fracture; but the added crack length would be achieved in relatively so few cycles that the total number of cycles to failure is not increased appreciably. It must be emphasized, however, that, while this conclusion is valid for the small, initially unnotched specimens conventionally used in low-cycle-fatigue tests, it may not be directly applicable to larger structures, especially if they contain flaws or notches.

Use of the crack-growth power laws does result in the possibility of deriving a power law for cyclic life in terms of plastic strain (or, in fact, in terms of stress range), but the implied exponents are not in complete agreement with the observed values. Part of this discrepancy may be due to the simplifications assumed in the derivation, but it may also be that the very process of studying crack-growth rates in small specimens, where the value of the actual applied strain becomes beclouded once the crack is large enough to take meaningful measurements, constitutes part of the difficulty. This problem requires further attention.

Item (5) of Table 6 points out that, when stage II cracking is involved, a linear life-fraction rule should not be expected to apply. The failure of the linear damage rule in such applications has not been discussed here but is well known from the literature. Thus, cases that involve an appreciable portion of the life in stage II cracking—for example, bending

tests, or those of large structures, especially if they contain notches or flaws—should not be expected to follow a linear damage rule. One of the most important reasons for the failure of the rule [item (6)] is the possibility of introducing important residual stresses when cracks are present, whereas such stresses are not considered in the conventional application of the theory. Other reasons, however, also operate. One is the nature of the crack-growth curve, as discussed in connection with Fig. 48; another is the life value used in the denominator of the cycle ratios, as discussed in connection with Fig. 49. The subject of cumulative fatigue damage of notched structures is a most important one and is receiving a great deal of attention in many laboratories at the present time.

Final Fracture

Although the fracture process is one of generating and propagating a crack, the fatigue life is usually taken as the number of cycles at which fracture occurs. Final fracture is, however, a complex subject in itself. Most of the studies currently under way and the concepts that have been derived from them involve the assumption of linear elasticity in the major section of the body that undergoes fracture. The specimens from which our concepts of low- and intermediate-cycle fatigue are derived involve large plastic strains, usually throughout the fracture cross section. Thus, much needs to be done to bridge the gap between studies of fatigue and of fracture and hopefully this subject will constitute much of the content of those reports identified in Fig. 1 by the dashed curve.

Acknowledgment

In conclusion, I wish to express deep gratitude to my co-workers whose careful experiments and helpful discussions have been of the utmost value in the preparation of this report: M. H. Hirschberg, W. B. Bedesem, J. C. Freche, C. R. Ensign and J. R. Kubancik.

References

1. *Thompson, N., and Wadsworth, N. J., "Metal Fatigue," Advances in Physics (Supplement to Phil. Mag.), 7, 72–169 (1958).*
2. *Alden, T. H., "Basic Studies of Fatigue Fracture in Pure Metals," Rpt No. 62-RL-2923M, General Electric Rsch. Lab., (Feb. 1962).*
3. *Avery, D. H., and Backofen, W. A., "Nucleation and Growth of Fatigue Cracks," in Fracture of Solids, ed. by D. C. Drucker and J. J. Gilman, John Wiley & Sons, Inc., N. Y. (1963).*
4. *Grosskreutz, J. C., "A Critical Review of Micromechanisms in Fatigue," Proc. 10th Sagamore Army Mtls. Rsch. Conf., in Fatigue—An Interdisciplinary Approach, ed. by J. J. Burke, N. L. Reed and V. Weiss, Syracuse University Press, 27–59 (1964).*
5. *Gerberich, W. W., "Plastic Strains and Energy Density in Cracked Plates. I. Experimental Techniques and Results," GALCITSM 63-23, Graduate Aeronautical Labs., California Institute of Technology, Pasadena, Calif. (June 1963).*
6. *Oppel, G. U., and Hill, P. W., "Strain Measurements at the Root of Cracks and Notches," EXPERIMENTAL MECHANICS, 4 (7), 206–211 (1964).*
7. *Howie, A., and Whelan, M. J., "Diffraction Contrast of Electron Microscope Images of Crystal Lattice Defects," Proc. Royal Soc. London, A263, 217–237 (1961).*
8. *Grosskreutz, J. C., "Research on the Mechanisms of Fatigue," Tech. Documentary Rpt No. WADD-TR-60-313, pt. II, Prepared under Contract No. AF 33(616)-7858 by Midwest Rsch. Institute (Dec. 1963).*
9. *Bassett, G. A., Menter, J. W., and Pashley, D. W., "Moiré Patterns on Electron Micrographs, and Their Application to the Study of Dislocations in Metals," Proc. Royal Soc. London, A246, 345–368 (1958).*
10. *Lang, A. R., "Studies of Individual Dislocations in Crystals by X-ray Diffraction Microradiography," Jnl. Appl. Physics, 30, 1748–1755 (1959).*
11. *Dash, W. C., "The Observation of Dislocations in Silicon," Dislocations and Mechanical Properties of Crystals, John Wiley & Sons, Inc., New York, 57–67 (1957).*
12. *Hahn, G. T., and Rosenfield, A. R., "Local Yielding and Extension of a Crack under Plane Stress," Battelle Memorial Inst. (1964).*
13. *Wood, W. A., Cousland, S. McK., and Sargent, K. R., "Systematic Microstructural Changes Peculiar to Fatigue Deformation." Acta Metallurgica, 11, 643–652 (1963).*
14. *Smith, R. W., Hirschberg, M. H., and Manson, S. S., "Fatigue Behavior of Materials Under Strain Cycling in Low and Intermediate Life Range," NASA TN D-1574 (Apr. 1963).*
15. *Manson, S. S., and Hirschberg, M. H., "Fatigue Behavior in Strain Cycling in the Low and Intermediate Cycle Range," Fatigue—An Interdisciplinary Approach, ed. by J. J. Burke, N. L. Reed and V. Weiss, Syracuse University Press, 133–173 (1964).*
16. *Manson, S. S., "Behavior of Materials Under Conditions of Thermal Stress," Heat Transfer Symp., University of Michigan, June 27–28, 1952, University of Michigan Press. Also: Manson, S. S., "Behavior of Materials Under Conditions of Thermal Stress," NACA TN 2933 (July 1953).*
17. *Manson, S. S., "Thermal Stresses in Design, Part 19—Cyclic Life of Ductile Materials," Machine Design, 139–144 (July 7, 1960).*
18. *Laird, C., and Smith, G. C., "Initial Stages of Damage in High Stress Fatigue in Some Pure Metals," Phil. Mag., 8, 1945–1963 (Nov. 1963).*
19. *Coffin, L. F., Jr., "A Study of the Effects of Cyclic Thermal Stresses on a Ductile Metal," Trans. ASME, 76, 931–950 (1954).*
20. *Weiss, V., "Analysis of Crack Propagation in Strain-Cycling Fatigue," in Fatigue—An Interdisciplinary Approach, ed. by J. J. Burke, N. L. Reed and V. Weiss, Syracuse University Press, 179–186 (1964).*
21. *Palmgren, A., "Die Lebensdauer von Kugellagern," ZVDI, 68 (14), 339–341 (Apr. 1924).*
22. *Langer, B. F., "Fatigue Failure from Stress Cycles of Varying Amplitudes," Jnl. Appl. Mech., 4 (4), A160–A162 (1937).*
23. *Miner, M. A., "Cumulative Damage in Fatigue," Ibid., 12, A159–A164 (1945).*
24. *Grover, H. J., "An Observation Concerning the Cycle Ratio in Cumulative Damage," Symp. on Fatigue of Aircraft Structures, ASTM, STP No. 274 (1960).*
25. *Manson, S. S., Nachtigall, A. J., and Freche, J. C., "A Proposed New Relation for Cumulative Fatigue Damage in Bending," Proc. ASTM, 61, 679–703 (1961).*
26. *Manson, S. S., Nachtigall, A. J., Ensign, C. R., and Freche, J. C., "Further Investigation of a Relation for Cumulative Damage in Bending." NASA Tech. Memo. TM X-52002 (1964).*
27. *Weibull, W., "The Effect of Size and Stress History on Fatigue Crack Initiation and Propagation," Proc. Crack Propagation Symp., Cranfield, 271–286 (1961).*
28. *Richart, F. E., Jr., and Newmark, N. M., "An Hypothesis for the Determination of Cumulative Damage in Fatigue," Proc. ASTM, 48, 767–800 (1948).*
29. *Kaechele, L. E., "Review and Analysis of Cumulative Fatigue Damage Theories," The Rand Corp., RM-3650-PR (1963).*
30. *Corten, H. T., and Dolan, T. J., "Cumulative Fatigue Damage," Paper No. 2 of Session 3, Intl. Conf. on Fatigue of Metals, 1, Inst. Mech. Engrs., London (1956).*
31. *Freudenthal, A. M., and Heller, R. A., "Accumulation of Fatigue Damage," Fatigue of Aircraft Structures, Academic Press, Inc., N. Y., 146–177 (1956).*
32. *Freudenthal, A. M., and Heller, R. A., "On Stress Interaction in Fatigue and a Cumulative Damage Rule: Part I—2024 Aluminum and SAE 4340 Steel Alloys," WADC TR 58-69, 1958 (AD 155687).*
33. *Henry, D. L., "A Theory of Fatigue-Damage Accumulation in Steel." Trans. ASME, 77, 913–918 (1955).*
34. *Gatts, R. R.: "Application of a Cumulative Damage Concept to Fatigue," Trans. ASME, Series D, Jnl. Basic Engrg., 83D (4), 529–540 (1961).*
35. *Brown, G. W., and Work, C. E., "An Evaluation of the Influence of Cyclic Prestressing on Fatigue Limit," Proc. ASTM, 63, 706–716 (1963).*
36. *Grover, H. J., "Cumulative Damage Theories," Fatigue of Aircraft Structures, WADC Symp., WADC, TR 59-507, 207–225 (Aug. 1959).*
37. *Morrow, J., and Johnson, T. A., "Correlation Between Cyclic Strain Range and Low-Cycle Fatigue Life of Metals," Mtls. Rsch. & Stds., 5 (1), 30–32 (1965).*
38. *Peterson, R. E., "A Method of Estimating the Fatigue Strength of a Member Having a Small Ellipsoidal Cavity," Intl. Conf. on Fatigue of Metals, Inst. Mech. Engrs., London, 110–117 (1956).*
39. *Ronay, M., "On Strain Incompatibility and Grain Boundary Damage in Fatigue," Columbia Univ., Inst. for the Study of Fatigue and Reliability, Tech. Rpt. No. 9 (Aug. 1964).*
40. *McEvily, A. J., Jr., and Boettner, R. C., "A Note on Fatigue and Microstructure," Fracture of Solids, John Wiley & Sons, N. Y., 383–389 (1963).*
41. *Wood, W. A., "Recent Observations on Fatigue Failure in Metals," ASTM STP No. 237, 110–119 (1958).*
42. *Schijve, J., "Analysis of the Fatigue Phenomenon in Aluminum Alloys," Natl. Aero- and Astronautical Rsch. Inst., Amsterdam, NLR-TR-M2122 (1964).*
43. *Forsyth, P. J. E., "A Two-Stage Process of Fatigue-Crack Growth," Proc. Crack Propagation Symp., Cranfield, 76–94 (1961).*
44. *Laird, C., and Smith, G. C., "Crack Propagation in High Stress Fatigue," Phil. Mag., 7, 847–857 (1962).*